AD-A060 548 AIR FORCE MATERIALS LAB WRIGHT-PATTERSON AFB OHIO F/G 11/4
FATIGUE BEHAVIOR AND LIFE PREDICTION OF COMPOSITE LAMINATES.(U)
APR 78 H T HAHN

UNCLASSIFIED AFML-TR-78-43 NL

| OF |
AD
A060548

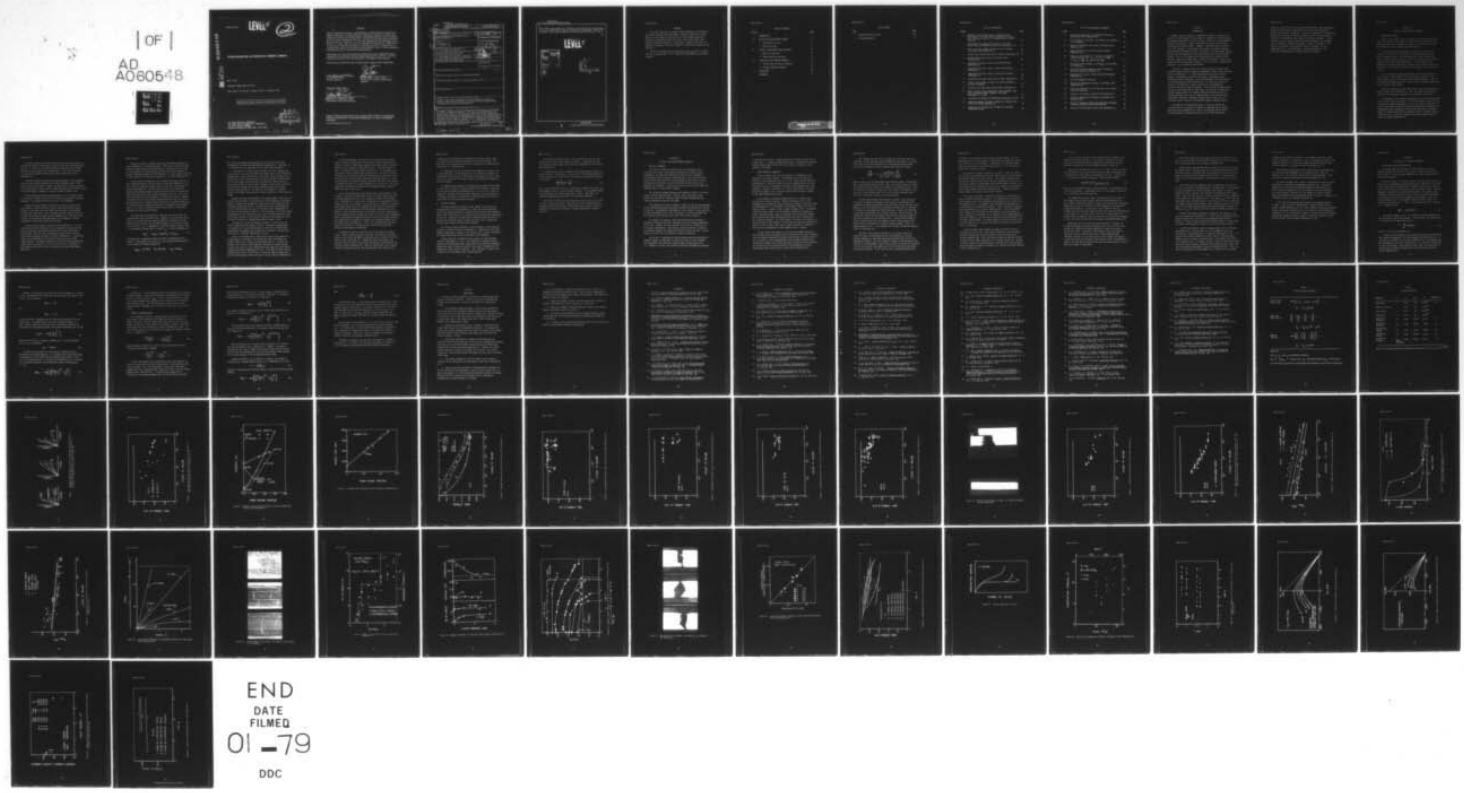

END
DATE
FILMED
01-79
DDC

AFML-TR-78-43

LEVEL II

AD A060548

DDC FILE COPY

FATIGUE BEHAVIOR AND LIFE PREDICTION OF COMPOSITE LAMINATES

April 1978

TECHNICAL REPORT AFML-TR-78-43

Final Report for Period 1 October 1977 to 31 January 1978.

Approved for public release; distribution unlimited.

DDC
RECEIVED
OCT 31 1978
D

AIR FORCE MATERIALS LABORATORY
AIR FORCE WRIGHT AERONAUTICAL LABORATORIES
AIR FORCE SYSTEMS COMMAND
WRIGHT-PATTERSON AIR FORCE BASE, OHIO 45433

78 10 23 002

NOTICE

When Government drawings, specifications, or other data are used for any purpose other than in connection with a definitely related Government procurement operation, the United States Government thereby incurs no responsibility nor any obligation whatsoever; and the fact that the government may have formulated, furnished, or in any way supplied the said drawings, specifications, or other data, is not to be regarded by implication or otherwise as in any manner licensing the holder or any other person or corporation, or conveying any rights or permission to manufacture, use, or sell any patented invention that may in any way be related thereto.

This report has been reviewed by the Information Office (ASD/OIP) and is releasable to the National Technical Information Service (NTIS). At NTIS, it will be releasable to the general public, including foreign nations.

This technical report has been reviewed and is approved for publication.

H. THOMAS HAHN
Project Engineer

STEPHEN W. TSAI, Chief
Mechanics & Surface Interactions Branch

FOR THE DIRECTOR

JEROME M. KELBLE, Chief
Nonmetallic Materials Division

Copies of this report should not be returned unless return is required by security considerations, contractual obligations, or notic on a specific document.

AIR FORCE/56780/25 September 1978 — 200

UNCLASSIFIED

SECURITY CLASSIFICATION OF THIS PAGE *(When Data Entered)*

REPORT DOCUMENTATION PAGE		READ INSTRUCTIONS BEFORE COMPLETING FORM
1. REPORT NUMBER AFML-TR-78-43	2. GOVT ACCESSION NO.	3. RECIPIENT'S CATALOG NUMBER
4. TITLE *(and Subtitle)* FATIGUE BEHAVIOR AND LIFE PREDICTION OF COMPOSITE LAMINATES		5. TYPE OF REPORT & PERIOD COVERED Final Report 1 Oct 77 - 31 Jan 78 6. PERFORMING ORG. REPORT NUMBER
7. AUTHOR(s) H. Thomas Hahn		8. CONTRACT OR GRANT NUMBER(s) 74 pp.
9. PERFORMING ORGANIZATION NAME AND ADDRESS Air Force Materials Laboratory Air Force Wright Aeronautical Laboratories, AFSC Wright-Patterson AFB, Ohio 45433		10. PROGRAM ELEMENT, PROJECT, TASK AREA & WORK UNIT NUMBERS 2419 [redacted] 2307 [redacted] 03
11. CONTROLLING OFFICE NAME AND ADDRESS Air Force Materials Laboratory (AFML/MBM) Air Force Wright Aeronautical Laboratories Wright-Patterson AFB, Ohio 45433		12. REPORT DATE Apr [redacted] 78 13. NUMBER OF PAGES 70
14. MONITORING AGENCY NAME & ADDRESS *(if different from Controlling Office)*		15. SECURITY CLASS. *(of this report)* Unclassified 15a. DECLASSIFICATION/DOWNGRADING SCHEDULE

16. DISTRIBUTION STATEMENT *(of this Report)*

Approved for public release, distribution unlimited. 62102F

17. DISTRIBUTION STATEMENT *(of the abstract entered in Block 20, if different from Report)*

18. SUPPLEMENTARY NOTES

19. KEY WORDS *(Continue on reverse side if necessary and identify by block number)*

Fatigue, Failure mode, Temperature increase, Damage rate, Composite laminates, Fatigue notch sensitivity, Frequency effect, Modulus change, Life prediction, Statistical data analysis.

20. ABSTRACT *(Continue on reverse side if necessary and identify by block number)*

This report presents a survey of some of the available data on the effects of fatigue in composite laminates. Both static and fatigue behaviors of unidirectional laminae are discussed in terms of the static failure and fatigue limit strains of the constituents as well as of the loading conditions. Subcritical failure modes in multidirectional laminates are delineated and correlated with the material responses such as temperature increase, modulus change, and fatigue notch insensitivity. Also included are the effects of

DD FORM 1 JAN 73 1473 EDITION OF 1 NOV 65 IS OBSOLETE

UNCLASSIFIED

SECURITY CLASSIFICATION OF THIS PAGE *(When Data Entered)*

012 320 78 10 23 002

test frequency and compression. Methods of predicting the fatigue strengths of off-axis laminae and of angle-ply laminates are summarized. Finally, two statistical life prediction models are discussed using the material "age".

LEVEL II

ACCESSION for
NTIS White Section
DDC Buff Section
UNANNOUNCED
JUSTIFICATION
BY
DISTRIBUTION/AVAILABILITY CODES
Dist. AVAIL. and/or SPECIAL
A

DDC
RECEIVED
OCT 31
D

FOREWORD

This report describes an inhouse effort conducted in the Mechanics and Surface Interactions Branch (MBM), Nonmetallic Materials Division (MB), Air Force Materials Laboratory, Air Force Wright Aeronautical Laboratories, Wright-Patterson AFB, Ohio, under Project 2419, "Nonmetallic Structural Materials", Task 241903, "Composite Materials and Mechanics Technology", Work Unit 23190310, "Durability of Composites and Adhesives."

The work reported herein was performed during the period 1 October 1977 to 31 January 1978. Dr. H. Thomas Hahn (AFML/MBM) was the project engineer.

TABLE OF CONTENTS

SECTION		PAGE
I	INTRODUCTION	1
II	FATIGUE IN UNIDIRECTIONAL LAMINAE	3
	1. Longitudinal Fatigue	3
	2. Off-Axis Fatigue	8
III	FATIGUE IN MULTIDIRECTIONAL LAMINATES	10
	1. Angle-Ply Laminates	10
	2. Fiber-Controlled Laminates	11
IV	STATISTICAL LIFE PREDICTION MODELS	17
	1. Failure Rate and Failure Potential	17
	2. Strength Degradation Model	19
V	CONCLUSIONS	22
	REFERENCES	24

PRECEDING PAGE NOT FILMED
BLANK

LIST OF TABLES

TABLE		PAGE
1	Fatigue Failure Functions	30
2	Fatigue Parameters	31

LIST OF ILLUSTRATIONS

FIGURE		PAGE
1	Schematic Stress-Strain Curves of Composites and Constituents: (a) Metal Matrix Composites; (b) Glass Fiber Reinforced Plastics; (c) Advanced Polymer Matrix Composites.	32
2	Longitudinal S-N Data, B/Al and BSiC/Ti (UTS=1698 MPa for B/Al and 1296 MPa for BSiC/Ti) (References 7, 9)	33
3	Effects of Fiber Volume Fraction on Static Strength and Fatigue Limit (Reference 7).	34
4	Fatigue Limit Predicted by Rule of Mixtures (Reference 25).	35
5	Maximum Strain versus Cycles to Failure, Gl/Ep (Reference 29).	36
6	Longitudinal S-N Data, Type I Gr/Ep (UTS=872 MPa) (Reference 30).	37
7	Longitudinal S-N Data, Type II Gr/Ep (UTS=1345 MPa) (Reference 31).	38
8	Longitudinal S-N Data, Type III Gr/Ep (UTS=1732 MPa) (Reference 31).	39
9	Longitudinal S-N Data, B/Ep (UTS=1331 MPa) (Reference 3).	40
10	Typical Failure Modes of Gr/Ep: (a) Strong Interphase (b) Weak Interphase.	41
11	Transverse S-N Data, B/Ep (UTS=60.9 MPa) (Reference 3).	42
12	Shear S-N Data, B/Ep (Longitudinal Shear Strength = 66.7 MPa, Interlaminar Shear Strength = 81.4 MPa) (References 3, 5, 42).	43
13	Predictions of Off-Axis S-N Relations (References 43, 45).	44
14	Comparison Between Strengths of Angle-Ply Laminates and Off-Axis Strength (Reference 47).	45
15	Predictions of S-N Relations of Angle-Ply Laminates (References 43,46).	46

LIST OF ILLUSTRATIONS (CONTINUED)

FIGURE		PAGE
16	Stress-Strain Relations of $(0/\pm45/90)_s$ Gl/Ep and of Constituent Plies (Reference 54).	47
17	Failure Modes at Free Edge: (a) $(0/90)_s$; (b) $(0/\pm45)_s$; (c) $(0/\pm45/90)_s$.	48
18	Number of Transverse Cracks Versus Laminate Stress (Reference 52).	49
19	Damage Indications in Cross-Ply Gl/Ep Laminate (Reference 55).	50
20	Change of Secant Modulus in Fatigue of $(0/\pm45/90)_s$ Gl/Ep (Reference 54). S_{max} = 62 (o), 103 (●), 138 (◆), 172 (▼), 207 (■), 248 MPa (▲).	51
21	Macroscopic Failure Modes: (a) $(0/90)_{2s}$; (b) $(0/\pm45)_s$; (c) $(0/\pm45/90)_s$.	52
22	Static and Fatigue Strengths of Fiber-Controlled Laminates (Data from Reference 3).	53
23	Normalized S-N Curves of Fiber-Controlled Laminates (Reference 3).	54
24	Typical Temperature Increase.	55
25	Equilibrium Temperature Increase, $(0/\pm45/90)_s$ Gl/Ep (Reference 54).	56
26	Effect of Frequency f in Hz on Fatigue Life, $(0/\pm45)_s$ Gr/Ep (Reference 60).	57
27	Constant Life Diagram, $(0_3/\pm45)$ B/Ep (Reference 3).	58
28	Effect of Compression on Fatigue, $(0/\pm45/90)$ Gr/Ep (Reference 66).	59
29	Effect of Fatigue on Tensile and Compressive Residual Strengths $(0/\pm45/90)$ Gr/Ep (Reference 66).	60
30	Inverse of Fatigue Notch Factor, B/Ep (Reference 3).	61

SECTION I

INTRODUCTION

Whereas fatigue in metals is understood in terms of nucleation and growth of a single dominant flaw, fatigue in composites is characterized by initiation and growth of multiple cracks. Because of the heterogeneity inherent in composites, cracks in composites no longer have the same implications as those in metals. Damage in composites can be any one or all of the following: fiber breaks, resin cracks, interfacial debonds, and delaminations between the plies of laminate. All these cracks are not separate but interconnected, making identification of crack paths highly complex. Much of this damage occurs long before the ultimate failure, and hence, there can be many types of subcritical failures. Each failure should be clearly defined and assessed in its criticality, if engineering designs are to be economical and reliable.

The class of composites that has received extensive fatigue study during the early stage of composites development is glass fiber reinforced plastics (References 1, 2). With the advent of new types of fibers, however, a good amount of work has been done on composites such as boron/epoxy (B/Ep) (References 3, 4), graphite/epoxy (Gr/Ep) References 5, 6), boron/aluminum (B/Al) (References 7, 8), and Borsic/titanium (B-SiC/Ti) (Reference 9). Data in the form of S-N diagrams are available for various types of loadings: axial tension and compression; in-plane, interlaminar and torsional shear; and flexure. Monitoring of fatigue damage by means of a number of NDE and DE techniques has improved considerably our level of understanding of failure mechanisms. Furthermore, seemingly incongruous fatigue data can now be put in a tractable form by using the life prediction models proposed recently.

The objective of the present report is to survey some of the available data on the effects of fatigue in composites and to discuss pertinent failure mechanisms in light of the observed failure modes. Since advantages of composites are found in the fiber-controlled

properties, both static and fatigue failure mechanisms under longitudinal loadings are discussed in some detail for unidirectional composites including metal matrix composites. A review is presented of the analytical methods for prediction of off-axis fatigue strength of unidirectional lamina and is extended to cover those for angle-ply laminates. Typical subcritical failure modes in multidirectional laminates are correlated with the changes in strength and modulus. Effects of frequency, compression, and notches are discussed in terms of fatigue life and temperature rise. A brief summary of recent developments in life prediction methodology then concludes the present report.

SECTION II

FATIGUE IN UNIDIRECTIONAL LAMINAE

1. LONGITUDINAL FATIGUE

Typical stress-strain curves of composites reinforced with brittle fibers to be discussed are shown in Figure 1 together with those of the constituent materials. Depending on the ductility and failure strain, those composites can be divided into three groups.

The first group typically exhibits the stress-strain curves of Figure 1(a) and consists of metal matrix composites reinforced with boron or graphite fibers. The second group is characterized by the fiber and matrix having almost the same failure strain (Figure 1(b)) and represents glass fiber reinforced plastics. Most polymer matrix composites reinforced with boron or graphite fibers belong to the third group which is distinguished from the first group by the low ductility of matrix.

Thus, in composites under consideration, fibers break before the matrix failure. What happens after a fiber breaks depends on many factors other than just the matrix and interphase properties. Some of the pertinent parameters and their effects on the subsequent damage mode are discussed in what follows.

The crack created by a fiber break tends to grow into the matrix at higher loading rate (Reference 10). Thus, the composite strength may decrease with increasing loading rate, as reported in Reference 11.

The subsequent crack growth also depends on the level of the applied stress at which the fiber breaks. If the fiber breaks at low stress due to defects or weakness (References 12, 13), the crack is more likely to lead to interfacial debond than to extend into the matrix (Reference 11). Consequently, when a composite contains many weak fibers, substantial number of fibers break before the composite failure. However, when the fibers are strong, a few fiber breaks seem enough to precipitate the composite fracture (Reference 14).

A similar behavior is observed at pre-existing fiber ends; that is, interfacial failure is more likely to occur at the fiber ends (References 14, 15). In fact, this difference between the pre-existing fiber ends and the new fiber breaks due to loading makes it possible to increase the composite strength by breaking weak fibers before fabrication (Reference 13).

Scattered, random fiber breaks manifest themselves in the dependence of the failure surface characteristics on the specimen length. Since there are more fiber breaks in longer specimens than in shorter specimens at the same level of applied stress, longer specimens tend to exhibit brush-like failure mode as compared to shorter specimens (Reference 16).

The foregoing observations are applicable in static tension as well as in fatigue. However, discussion of fatigue failure requires one more parameter - the fatigue sensitivity of matrix and interphase.

Composite fatigue behavior can best be correlated to that of the constituents in terms of fatigue strains rather than fatigue stresses because, in the fiber direction, both fibers and matrix are subjected to almost the same strain. Thus, although the actual state of stress is triaxial and includes residual stresses (References 17, 20), the following discussion should be understood within the framework of uniform longitudinal strain unless otherwise mentioned.

Figure 2 shows a typical S-N data of B/Al (Reference 21). As compared to boron fibers (Reference 22), the composite is seen to be more fatigue sensitive, indicating the possibility of matrix-controlled crack growth. Both the static strength and fatigue limit at various fiber volume fractions are shown in Figure 3 (Reference 7). The fatigue ratios in the parentheses are relatively insensitive to the fiber volume fraction. The lowest fatigue ratio at v_f=0.25 may be because the stress ratio is 0.2 while it is 0.4 at v_f=0.4 and 0.6. Decrease of the fatigue ratio with the stress ratio can also be seen from Figure 2 where R=0.

The matrix failure in fatigue can easily be detected through microscopic examinations of fracture surfaces. While static tensile fracture surfaces of B/Al maintain the characteristics of ductile fracture, such as voids formation, fatigue fracture surfaces exhibit some evidence of fatigue hardening and shear failure (Reference 7). Crack growth striations are also observed if the fibers are ductile, e.g., Be/Al (Reference 23).

Fatigue cracks in composites can initiate at the free surface as in metals and additionally, at fiber breaks or fiber ends (References 7, 9, 24). Fibers can break at stresses as low as half the ultimate tensile strength (Reference 24). Brittle coatings such as SiC and brittle reaction zones between fibers and matrix are more prone to cracking and effectively reduce the fiber strength (References 25, 26). Thus, more fiber fractures occur during fatigue in B-SiC/Al than in B/Al. However, the fatigue limit is only slightly reduced because the low yield stress and high ductility of aluminum allows the matrix to yield more readily in the fiber direction, thereby relieving stress concentration on adjacent fibers. As a result, deleterious planar crack growth is interrupted frequently by jogs along the fibers.

At higher fiber volume fraction, there are more fiber breaks and and hence more crack initiation sites. However, at the same time, more fibers act as crack arresters and more effective retardation of crack growth will be realized. The net effect appears to be that the fatigue limit in strain, ε_{FL}, is independent of the fiber volume fraction. That is, the composite fatigue limit in stress, S_{FL}, is given by Reference 27.

$$S_{FL} = S_{mFL} + v_f(E_f/E_m - 1)E_m \varepsilon_{FL} \qquad (1)$$

The prediction is compared with the data taken from Reference 25 in Figure 4. The fatigue limit strain ε_{FL} was calculated from the data at v_f=0.5 using the following properties:

$$S_{mFL} = 111 \text{ MPa}, \quad E_f = 400 \text{ GPa}, \quad E_m = 69 \text{ GPa}.$$

As is clear, the moduli were assumed not to be affected by fatigue although small decrease has been observed (Reference 25). Note that ε_{FL} is 0.36% which is well above the initial yield strain of 6061 Al.

If the matrix is strong in both stiffness and yield strength, yet highly ductile, the stress transfer from broken fibers to the neighboring unbroken ones is more effective and the fracture surface becomes fairly planar with no sign of longitudinal cracking in the matrix (Reference 9). For the same reason, the possibility of interfacial debond increases. Since fiber failure is brittle when it happens, the net effect can be an increased crack growth rate and the composite becomes more fatigue sensitive than the matrix. An example of such behavior is shown in Figure 2 for B-SiC/Ti which has poor fatigue resistance in the high-cycle region.

Fatigue in Gl/Ep, which belongs to the second group, Figure 1(b), is similar to that in B/Al in that the matrix itself undergoes a substantial damage in fatigue and consequently, fatigue cracks are observed at the free edges (References 28, 29). Fatigue limit strain of the composite is only slightly higher than that of the epoxy itself independently of the fiber volume fraction (Figure 5). The microcracks in the matrix grows perpendicular to the loading until they start to branch along the fibers. The ultimate fracture is the result of reduction in the effective cross-sectional area when the aforementioned process repeats itself.

In composites of the third group, the matrix is well within the elastic range up to the composite failure. Therefore, fatigue damage in the matrix will be negligible except at the sites of fiber breaks. Consequently, the modulus and strength do not decrease in fatigue until the fracture is imminent (References 4, 30, 31).

Since, for the same matrix, lower fiber failure strain means less fatigue damage in the matrix, the stiffer the fiber, the higher the fatigue ratio will be, Figures 6-8 (References 30, 31). In fact, the fatigue limit of Type I Gr/Ep composite, which has an average failure strain of only 0.5%, is only slightly below the lower tail end of static strength distribution (References 30, 32). Since Type III fiber has the largest failure strain of the three, it gives the lowest fatigue ratio. Note that B/Ep behaves similarly to Type II Gr/Ep, Figure 9 (Reference 3).

Failure mode depends very much on the interfacial bond strength. Figure 10 shows two contrasting failure modes of Gr/Ep; Figure 10(a) is typical of surface treated fiber composites and Figure 10(b) of surface untreated fiber composites (References 30, 34). The failure mode of B/Ep is in between the two extremes (Reference 4). In the former case, the fracture surface exhibits the characteristics of a brittle fracture originating at a very small group of fibers whereas in the latter, long slivery fractures indicate weak interfacial bond (Reference 32). Also, the macroscopic failure modes remain essentially the same as the loading is changed from static to fatigue (References 4, 30, 32, 33). Thus, the subcritical failure events leading to the ultimate fracture seem to be almost the same in both cases.

For all the differences in the failure mode, the difference in the strength is surprisingly negligible not only in static tension but also in fatigue (References 30, 32, 34). Composite failure can be thought of as a combination of fiber bundle failure and crack propagation failure neither of which is an optimum. As the interfacial strength is increased, fiber breaks dispersed in the longitudinal direction are isolated from one another and the composite strength increases (References 35, 36). However, if the interfacial bond is too strong, the stress concentration on the neighboring fibers becomes more effective, and the crack propagation mode will dominate the composite fracture, resulting in reduced strength. An optimum value of interfacial strength exists somewhere between these two extreme cases (Reference 37). Thus, it is possible that two equal composite strengths are realized on each side of the optimum bond although failure modes are different.

Longitudinal cracking is possible even in the absence of broken fibers. Under a tensile loading in the fiber direction, the circumferential stress at the fiber-matrix interface can be as large as 9% of the applied stress (Reference 17). Coupled with the curing stress, the resultant stress is sufficient to cause longitudinal cracking before the specimen fracture (Reference 34). When this longitudinal crack extends through the thickness and into the end tab region, the induced stress

concentration may produce partial debonding of the tabs and the load is forced to be carried by the remaining part of the specimen. The additional stress may then be sufficient to fracture the remaining part and end the test (Reference 33).

As compared to the tensile failure, the compressive failure is not so well understood. Failed specimens usually show various degrees of longitudinal splitting and, in some cases, shear type of failure. When only a small amount of splitting is present, some degree of brooming is observed instead.

In graphite/epoxy composites the compressive strength can be higher or lower than the tensile strength depending on the material system and also on the test method used (References 5, 6, 34, 38, 39). Since the compressive strength of unidirectional composites is utilized better in a laminate, the effect of compression on fatigue behavior will be discussed later for multidirectional laminates.

2. OFF-AXIS FATIGUE

The fiber orientation relative to the loading axis affects the fatigue behavior in the same manner as it does the static properties; the off-axis fatigue behavior is controlled by the matrix and interphase unless fiber splitting occurs as observed in B/Al and B-SiC/Al (References 18, 40, 41). Especially in metal matrix composites where the matrix is ductile and interfacial bond is strong, both the static strength and fatigue limit increase with the matrix strength.

An S-N data of B/Ep subjected to tensile fatigue in the transverse direction is shown in Figure 11 (Reference 3). Compared with the longitudinal fatigue data of Figure 9, the fatigue ratio is lower, indicating the higher fatigue sensitivity of the matrix and interphase.

Similar reduction is observed in the fatigue of ($\pm$45) laminate, Figure 12 (References 3, 5, 42). This laminate is frequently used to determine the longitudinal shear properties of B/Ep and Gr/Ep composites because the elastic transverse stress is only about 20 percent of the longitudinal shear stress in each ply. Thus, the data of Figure 12 can be taken as the longitudinal shear fatigue behavior.

The transverse fatigue ratio is not much different from the longitudinal shear fatigue ratio (Figures 11 and 12). Furthermore, in B/Al the fatigue ratio was shown to be essentially independent of the off-axis angle (Reference 1).

In analogy to the static strength, several methods were proposed to predict off-axis S-N relations. In the main, all the methods make use of failure functions f_α so that failure occurs when the following condition is satisfied:

$$\max_{\alpha} \left\{ f_\alpha (\sigma_i, S_\beta) \right\} = 1 . \qquad (2)$$

Here σ_i are the applied stresses in the material symmetry axes and S_β are the parameters such as uniaxial fatigue strengths. The parameters depend on the fatigue cycles, but the functions f_α do not. Note that S_β-N relations should be obtained under similar loading conditions.

Three static failure functions have been tried so far f_α, as listed in Table 1 (References 43-46). Comparisons with the limited amount of available off-axis fatigue data indicate that one can expect as good an agreement in fatigue as in tension. A sample comparison is shown in Figure 13.

SECTION III

FATIGUE IN MULTIDIRECTIONAL LAMINATES

1. ANGLE-PLY LAMINATES

The effect of constraint between plies with different fiber orientations are best illustrated by comparing the ultimate tensile strengths of ($\pm\theta$) angle-ply laminates with the off-axis strength of unidirectional lamina, Figure 14 (Reference 47). The solid and broken lines represent the predictions by the maximum stress failure criterion and show the contributions of each constituent to the load carrying capability of laminates. Fibers are seen to carry more load in angle-ply laminates than in unidirectional laminae.

The constraint between adjacent plies manifests itself in the interlaminar stresses (Reference 48). However, these interlaminar shear stresses do not seem to influence fatigue strength although they may induce delamination along the free edges.

The prediction of static strength in Figure 14 requires the knowledge of the relationship between the applied laminate stresses and the stresses in each ply. Although the lamina behavior is not exactly linear especially in shear (References 49-52), this relationship is usually provided from the laminated plate theory based on the linear elastic behavior.

In fatigue, the problem is more complicated because the moduli, especially transverse and shear, decrease with cyclic loading (References 31, 48, 53). However, one can certainly use the elastic relations as a first-order approximation. Once the ply stresses are known in terms of the laminate stresses, an appropriate failure criterion in Table 1 can be chosen to predict the S-N relations of angle-ply laminates.

The results in References 44 and 46 indicate that the prediction of fatigue strength is comparable in accuracy to that of static strength. The experimental data exhibited slightly higher fatigue sensitivity, i.e., steeper S-N curves, than predicted and better agreement was observed

in the high cycle region. A sample comparison is shown in Figure 15 for a ($\pm$60) Gl/Ep. If complete delamination occurs, the strength of angle-ply laminate should reduce to that of off-axis lamina. However, no such reduction is observed.

2. FIBER-CONTROLLED LAMINATES

Figure 16 shows stress-strain relations of a $(0/\pm45/90)_s$ Gl/Ep subjected to a uniaxial tension. Superimposed are the stress-strain relations of the constituent plies, i.e., (0), ($\pm$45), and (90) laminates (Reference 54). Since the inplane strains are uniform from ply to ply, failure will occur in the weakest ply which is the 90-degree ply in the $(0/\pm45/90)_s$ laminate. Therefore, it is natural that cracks in tensile fatigue also appear first in the plies whose fiber direction is normal to the loading (References 55-59).

As an example, consider the damage process in a $(0/90)_s$ Gl/Ep subjected to a uniaxial tension. When the transverse stress in the 90-degree plies reaches the average transverse strength, transverse cracks form perpendicular to the loading in the 90-degree plies with a fairly regular spacing. A typical crack is shown in Figure 17(a). The maximum transverse stress, which is at the midpoint between two neighboring cracks, then drops down to about 73 percent of the transverse strength. Next cracking occurs when the maximum transverse stress reaches again the transverse strength. This time, however, the stress is reduced to a mere 27 percent of the strength. Since further cracking thus becomes more difficult, the existing cracks start to grow along the ply interfaces and the stress concentration on the 0-degree plies is reduced.

Figure 18 shows the number of cracks per unit length observed at the free edge and also permanent strain resulting from the crack formation. Large discrepancy between the prediction and the data at higher stresses is an indication of the aforementioned crack branching (Reference 52). The change of modulus also follows the pattern predicted from a reduction in the effective load carrying portion of the 90-degree plies when delamination grows from the tips of those cracks (Reference 49).

The 0-degree plies are also susceptible to cracking in the fiber direction. For the laminate under consideration, the ratio of the transverse stress σ_T^o in the 0-degree plies to the applied laminate stress N_x/h can be calculated from the laminated plate theory as follows:

$$\frac{\sigma_T^o}{N_x/h} = 2 \frac{\nu_{LT}(E_L E_T - E_T^2)}{(E_L + E_T)^2 - 4 \nu_{LT}^2 E_T^2} \tag{3}$$

where E_L and E_T are the longitudinal and transverse moduli, respectively, and ν_{LT} the major Poisson's ratio. Thus, in a typical Gl/Ep, the transverse stress can be as high as six percent of the laminate stress. Since the transverse strength is usually less than 35 MPa, longitudinal cracks can occur in the 0-degree plies of cross-ply S-glass laminates which have the longitudinal strength of more than 830 MPa.

The same failure modes are observed in fatigue. Even during the first cycle a number of transverse cracks appear in proportion to the exceedance of the maximum fatigue stress over the first ply failure stress. However, very little increase in the number of these cracks is observed in fatigue for the reasons described previously. Rather, the transverse cracks grow into delamination as fatigue proceeds. On the contrary, the longitudinal cracks in the 0-degree plies initiate, multiply gradually, and reach a plateau with the fatigue cycles. The equilibrium number of cracks (in both plies) does not change as long as those maximum transverse stresses are below the transverse fatigue strength. Also, the damage manifests itself in the reduction of residual strength and modulus, Figure 19 (Reference 55).

The static stress-strain relation of a cross-ply laminate is usually bilinear and represented by the initial modulus E_o and the secondary modulus E_b, the latter being approximately equal to half the longitudinal modulus. With the progress of damage in the 90-degree plies, the knee in the subsequent bilinear stress-strain curve moves up along the initial stress-strain curve above the first ply failure point and hence the modulus decreases. In the limiting case of complete delamination,

the modulus will be equal to half the longitudinal modulus. For the composite, which is S-glass/epoxy, (Figure 19) the experimental value of E_b is close to $E_L/2$, as predicted. Furthermore, the predicted modulus after the first cycle is not much higher than $E_L/2$. The data approximately falls within this range.

The behavior of $(0/\pm45)_s$ laminates is similar to that of unidirectional B/Al; the ±45-degree plies do not show any sign of failure before the laminate fracture in static tension. The reason is because (±45) laminate has higher failure strain than the longitudinal failure strain. In fatigue, however, the ±45-degree plies exhibit gradual cracking, just the same way as the 0-degree plies in cross-ply laminates do, because of their higher fatigue sensitivity (Reference 60). Figure 17(b) shows cracks produced in fatigue, not in static tension.

The failure mechanisms in (0±45/90) laminates are combinations of those in (0/90) and (0/±45) laminates. The sequence of ply failures is the 90-degree plies first followed by the ±45-degree plies, Figure 17(c) (References 54, 61). The damage in the ±45-degree and 90-degree plies is manifested in the decrease of modulus. Figure 20 shows the change of the secant modulus E_{sn} in fatigue (Reference 54). Since the 0-degree plies comprise only 25 percent of the laminate, the secant modulus at static fracture is accordingly low as compared to the tangent modulus E_o. The secant modulus E_{s1} at the start of fatigue naturally decreases with increasing fatigue stress. The secant modulus at fatigue failure can be less than that at static fracture and seems to increase as the fatigue stress is decreased.

Typical ultimate failure modes are shown in Figure 21 for the laminates discussed so far. Very little difference is observed macroscopically between the fracture surfaces in static tension and in fatigue (Reference 60). Also, the laminates that are fiber-controlled in static tension remain essentially so in fatigue (Figure 22). Because of the ply failures discussed previously, fatigue sensitivity increases with decreasing percentage of 0-degree plies, see the (0/±45/90) laminate, Figure 23 (Reference 3).

The ply failures as well as the viscoelasticity of polymer matrix generate heat within laminates. Three types of temperature rise are observed on the specimen surface, depending on the material system, laminate configuration, and the loading conditions (Figure 24).

The equilibrium temperature increase ΔT in Types 1 and 2 was shown to be predictable from a heat transfer analysis under the assumption of a constant rate of heat generation (References 54, 62). In particular, ΔT is related to the loading parameters in the following manner:

$$\Delta T \propto (1-R)^2 S_{max}(S_{max}-S_o)f , \qquad (4)$$

where S_o is the threshold stress below which there is no hysteresis and f is the test frequency. Experimental data for ΔT are shown in Figure 25 for a $(0/\pm 45/90)_s$ Gl/Ep (Reference 54).

The temperature rise was shown to change from Type 2 to Type 3 as the fatigue stress and the frequency were increased (Reference 62). Thus, higher frequency can result in shorter life because ever increasing temperature of Type 3 is indicative of the damage rate increasing with fatigue (Reference 62). In the case of Type 1 behavior the test frequency has only negligible effect on the life, Figure 26 (Reference 60). In this regard, it is interesting to note that in interrupted stress rupture tests the number of cycles to failure can increase with frequency in such a way that the time under load remains unchanged (Reference 63).

When weaker plies fail and lead to delamination in fatigue, the antibuckling support provided for 0-degree plies by the off-axis plies becomes less effective and hence compression, rather than tension, failure will result. Because of large diameter, B/Ep is stronger in compression than in tension under static loading (Reference 64). Therefore, the peak of a low cycle curve in the constant life diagram is observed in the negative mean stress quadrant, Figure 27 (Reference 3). However, the peak moves toward the positive mean stress quadrant as the high cycle region is approached.

On the other hand, most Gr/Ep composites are not stronger in compression even statically and the peaks of constant life curves invariably lie in the positive mean stress quadrant (Reference 65).

Another example showing the effect of compression is given in Figure 28 (Reference 66). The data points at 10^3 cycles are almost parallel to the broken line; an indication that the fatigue failure in the low cycle region is controlled by the maximum tensile stress. In the high cycle region the controlling parameter is the alternating stress or the stress range.

That fatigue has more damaging effect on compressive strength can also be seen in Figure 29 (Reference 66). Although there is no difference in static strength, the residual strength after fatigue is lower in compression than in tension, the difference increasing with the fatigue cycles. Note also that the cycle ratio has negligible effect as compared to the number of cycles endured itself. Thus, when S_{min} is well into the compression region, fatigue failure is more likely to occur in compression. For example, $(0_3/\pm 45)$ B/Ep showed no sign of decrease in tensile strength under fully reversed tension-compression fatigue although it failed in fatigue at S_{max} less than half the static tensile strength (Reference 3).

Perhaps, the biggest advantages of composites over metals is the very low fatigue notch sensitivity. In static tension $(0/\pm 45/90)_s$ Gr/Ep exhibits higher notch sensitivity than comparable aluminum 7075. However, in fatigue, notched composite laminates behave as if there were no notches, when compared in terms of net section fatigue strength.

The difference between crack tip damages under static and fatigue environments can clearly be shown in X-ray photographs taken after application of tetrabromoethane as a penetrant (References 67, 68). In a $(0/\pm 45)$ Gr/Ep laminate subjected to static tension, almost the same amount of matrix cracking is observed both in the 0-degree plies and in the ± 45-degree plies. In fatigue, the matrix cracks in the 0-degree plies grow much longer distances, sometimes even reaching the grip region, and the crack opening displacement increases (References 68-70). Thus, the stress concentration on the 0-degree plies is reduced and the residual

strength of the laminate increased. In the meantime, the net section fatigue increases as if there were no crack. The overall process is thus something like wear-in in the early stage, followed by wear-out later. A similar behavior is observed for holes (References 65, 71).

The foregoing observations are also borne out by the fatigue notch factor being almost independent of the fatigue cycles, Figure 30 (Reference 3). Fatigue notch insensitivity of Gr/Ep laminates is also realized in compression-dominated fatigue (References 72, 73).

The extensive damage near a notch is responsible for excessive heat generation, as detected by thermography (Reference 74). Since both temperature rise and hole opening displacement are manifestations of matrix-controlled properties, they will depend on the test frequency. Thus, when failure is defined as a fixed amount of increase in hole opening displacement, the corresponding fatigue life will, in general, be influenced by the test frequency (Reference 71).

So far, the discussion has been limited to the inplane uniaxial loadings. There is only a limited amount of data available for the biaxial fatigue (References 75, 76). Also, whereas the torsional fatigue displays the general characteristics of the matrix-controlled behavior (References 77, 78), the flexural fatigue is similar to the axial fatigue, provided the nonuniform state of stress is taken into account in interpreting the data from the former (References 29, 79).

SECTION IV

STATISTICAL LIFE PREDICTION MODELS

1. FAILURE RATE AND FAILURE POTENTIAL

As failure modes of composites are rather complex, statistical methods have been resorted to in the analysis and characterization of the life data. Failure processes hopefully are then inferred from the statistical parameters.

A failure process is often described by using the failure rate which physically is interpreted as the probability of a specimen failing within a unit time interval (Reference 80). Although the real time is usually used in the discussion of the failure rate, the material "age" τ has been proposed to replace the real time (Reference 43). This material age represents the aging of material just as the strain-hardening parameter is a measure of the plastically deformed state in metals. Next, the failure potential $\psi(\tau)$ is introduced so that the failure rate is its derivative with respect to τ. That is, the probability $R(\tau)$ of survival at τ is related to ψ by

$$R(\tau) = \exp\left[-\psi(\tau)\right] \tag{5}$$

The relation between ψ and τ is an intrinsic material property and the load history enters only through τ. In particular, the material age τ is related to the load history $\sigma(t)$ by

$$\tau = \int_0^t K(\sigma(\xi))d\xi \ , \tag{6}$$

where K is called the breakdown rule.

A power law was proposed for the failure potential and two different laws, power and exponential, for the breakdown rule (Reference 81). In the original formulation of the theory (Reference 81), the breakdown rule was independent of the type of load history; i.e., the same rule applied to every load hostory. These laws were later found to be applicable to unidirectional composites subjected to static tension and to static fatigue (Reference 82).

However, in the present discussion the original assumption is relaxed so that the breakdown rule remains the same only within each type of load history. Thus, we choose

$$\psi(\tau) = \tau^{\alpha} \tag{7}$$

and

$$K(\sigma) = c_1 \sigma^{\gamma} \tag{8}$$

in static tension. Breakdown rule for the fatigue loading will be discussed later. The probability of surviving the failure stress x in static tension, hereafter called the static strength distribution, is then given by a two-parameter Weibull distribution (References 43, 81, 82):

$$R_s(x) = \exp\left[-\left(\frac{x}{x_o}\right)^{\alpha_s}\right] . \tag{9}$$

Here the characteristic strength x_0 depends on c_1, γ and the loading rate, and α_s is defined by

$$\alpha_s = \alpha(\gamma+1) \tag{10}$$

In order to distinguish as much as possible between the static strength and the fatigue behavior, it is assumed that the fatigue loading is preceded by a static tension to the maximum fatigue stress. Then, in terms of the material age L in fatigue, the probability $R_f(L)$ of survival at L, hereafter called the life distribution, follows from Equations 6 - 8 as

$$R_f(L) = \exp\left\{-\left[\left(\frac{S_{max}}{x_o}\right)^{\gamma+1} + L\right]^{\alpha}\right\} \tag{11}$$

Equation 11 is a three-parameter Weibull distribution with a negative location parameter. $R_f(o)$ simply represents the probability of surviving the initial static tension to S_{max}. In fact, the possibility of a negative location parameter was indicated in the fatigue data of (0/±45/90) Gr/Ep (Reference 66). The relation between L and the fatigue cycles requires another breakdown rule. This will be discussed in the next subsection.

2. STRENGTH DEGRADATION MODEL

Since composite failure is characterized by a multitude of cracks rather than a single dominant crack growth, the residual strength is chosen in place of the crack length to describe the criticality of the damage. Nevertheless, the change of the residual strength is postulated in analogy to the crack growth laws in metals (References 83, 84). In terms of the material age, the change of the normalized residual strength x_r/x_o is assumed to be

$$\frac{d(x_r/x_o)}{dL} = -\frac{1}{\gamma+1}\left(\frac{x_r}{x_o}\right)^{-\gamma} \tag{12}$$

Upon integration, Equation 12 yields the relation between the static strength and the residual strength:

$$\left(\frac{x_r}{x_o}\right)^{\gamma+1} = \left(\frac{x}{x_o}\right)^{\gamma+1} - L \tag{13}$$

If the crack growth law is deterministic, the crack length at any time can be related to the initial length which in turn determines the static strength. Thus, one can establish a one-to-one relationship between the static strength and the fatigue life under a similar fatigue damage process (Reference 85). In unidirectional composites the similarity of the fatigue damage process has been established through

proof testing (References 33, 84). In other words, a specimen which is strong statically is also strong in fatigue. Therefore, if the static strength distribution is given by (cf. Equation 9)

$$R_s(x) = \exp\left[-\left(\frac{x}{x_o}\right)^{\alpha_s}\right] \tag{14}$$

the residual strength distribution $R_r(x_r)$ follows upon substitution of Equation 13 into Equation 14:

$$R_r(x_r) = \exp\left\{-\left[\left(\frac{x_r}{x_o}\right)^{\gamma+1} + L\right]^{\alpha_s/(\gamma+1)}\right\} \tag{15}$$

Since fatigue failure occurs when the residual strength reduces to S_{max}, the life distribution $R_f(L)$ is obtained by substituting S_{max} for x_r in Equation 15:

$$R_f(L) = \exp\left\{-\left[\left(\frac{S_{max}}{x_o}\right)^{\gamma+1} + L\right]^{\alpha_s/(\gamma+1)}\right\} \tag{16}$$

Note that Equation 16 is exactly equal to Equation 11 in light of the relation between α and α_s (Equation 10). However, it should be recalled that the static strength distribution follows from the failure potential and the breakdown rule in the failure potential model whereas it is assumed a priori in the strength degradation model.

Suppose the material age in fatigue is related to the number of fatigue cycles n through another power law (cf. References 43, 83, 86):

$$L = C_2 S_{max}^{\beta} n \tag{17}$$

Equation 17 then gives the life distribution in terms of the fatigue cycles endured:

$$R_f(n) = \exp\left\{-\left[\left(\frac{S_{max}}{x_o}\right)^{\gamma+1} + \frac{n}{n_o}\right]^{\alpha}\right\} \tag{18}$$

where

$$n_o S_{max}^{\beta} = \frac{1}{C_2} \tag{19}$$

If the fatigue stress is much smaller than the characteristic static strength, the first term inside the brackets can be neglected and a two-parameter Weibull distribution is recovered. Equation 19 is none other than the power law relating the characteristic life n_o to S_{max}. The slope β of the log n_o - log S_{max} relation is thus a measure of the material aging; the steeper the slope is, the more rapidly the material ages.

Typical values of the parameters α, β, γ are listed in Table 2. The equality between β and γ does not seem universally valid even when R=1. γ is larger than β in the unidirectional composites subjected to static fatigue (R=1) whereas the reverse is observed for the quasi-isotropic laminates. Note that γ=1 was also proposed for Equation 13 without statistical considerations (Reference 88).

The models discussed so far have been used rather as a method of data analysis. It remains to be seen how these models will work as a true life prediction method under different loading environments.

SECTION V

CONCLUSIONS

A review has been presented of the effects of constant amplitude fatigue in composite laminates. Several life prediction methods were included in the discussion. The main conclusions are summarized as follows.

1. The subsequent damage following a fiber fracture depends not only on the matrix and interphase properties but also on the loading rate and the stress at the fiber fracture. Whereas the interfacial failure is favored at pre-existing fiber ends, crack propagation into the matrix is more likely when a fiber breaks under load. Also, failure mode depends on the specimen gage length.

2. Whereas the longitudinal static strength is controlled by the fibers, the fatigue limit is dominated by the matrix. A strong matrix coupled with strong interphase may even render the composite more fatigue sensitive because of the increased crack growth rate resulting from brittle fracture of fibers.

3. The highest longitudinal strength is associated with the cumulative fiber fracture mode and is realized at an optimum bond strength. The brush-like failure mode becomes prevalent below the optimum bond strength and the crack propagation mode above it. However, the corresponding composite strengths can be equal to each other. Very little difference is observed macroscopically between the static and the fatigue failure mode.

4. The fatigue strengths of off-axis laminae and of angle-ply laminates can be predicted to the same extent as the static counterparts can.

5. Typical subcritical failures in multidirectional laminates are the ply failure and the delamination. When a ply fails statically, i.e., due to overloading, it is not susceptible to further cracking in fatigue. When the failure is entirely due to fatigue the ply undergoes an asymptotically increasing amount of cracking.

6. Fatigue damage in composite laminates manifests itself in the temperature increase and modulus change. Ever increasing temperature is an indication of the damage rate increasing with fatigue. The damage rate depends on the test frequency.

7. Composite laminates exhibit very low fatigue notch sensitivity because of the beneficial stress relaxation at notch tips.

8. Subcritical damage is more detrimental to compressive strength. However, the effects are not surprising.

9. The failure potential model and the strength degradation model lead to the same life distribution although the underlying assumptions are different.

10. It remains to be seen how the proposed statistical life prediction models will work under different load histories.

REFERENCES

1. K. Boller, Composite Materials: Testing and Design, ASTM STP 460, American Society for Testing and Materials, p. 217, 1969.

2. M. J. Salkind, Composite Materials: Testing and Design (Second Conference), ASTM STP 497, American Society for Testing and Materials, p. 143, 1972.

3. P. D. Shockey, J. D. Anderson, and K. E. Hofer, Technical Report AFML-TR-69-101, Vol. V, Air Force Materials Laboratory, 1970.

4. E. C. Durchlaub and R. B. Freeman, Technical Report AFML-TR-73-225 (Vol. II), Air Force Materials Laboratory, 1974.

5. Development of Engineering Data on the Mechanical and Physical Properties of Advanced Composite Materials, Technical Report AFML-TR-72-205, Parts I and II, Air Force Materials Laboratory, 1972 and 1974.

6. Structural Criteria for Advanced Composites, Vol. I, Summary and Vol. II Detailed Information, Technical Report AFFDL-TR-72-142, Vols. I and II, Air Force Flight Dynamics Laboratory, 1977.

7. K. D. Shimmin and I. J. Toth, in Failure Modes in Composites, The Metallurgical Society of the AIME, p. 357, 1973.

8. T. R. Hancock, Fatigue of Boron-Aluminum Composites, Technical Report AFML-TR-72-113, Air Force Materials Laboratory, 1972.

9. S. T. Scheirer and I. J. Toth, The Mechanical Behavior of Metal Matrix Composites, Technical Report AFML-TR-73-178, Air Force Materials Laboratory, 1973.

10. J. Mullin, J. M. Berry, and A. Gatti, Journal of Composite Materials, Vol. 2, pp. 82-103, 1968.

11. J. T. Ryder, "The Effect of Compressive Loading on the Fatigue Lifetime of Graphite/Epoxy Laminates," Quarterly Progress Report No. 2, Contract No. F33(615)77-C-5045, Air Force Materials Laboratory, 1977.

12. K. N. Street and J. P. Ferte, Proc. of the 1975 International Conference on Composite Materials, Vol. 1, The Metallurgical Society of the AIME, pp. 137-163, 1976.

13. G. J. Mills, G. Brown, and D. Waterman, Proc. of the 1975 International Conference on Composite Materials, Vol. 2, The Metallurgical Society of the AIME, pp. 222-246, 1976.

14. J. H. Steele and H. W. Herring, Failure Modes in Composites, The Metallurgical Society of the AIME, pp. 343-356, 1973.

REFERENCES (CONTINUED)

15. D. M. Schuster and E. Scala, Fundamental Aspects of Fiber Reinforced Plastic Composites, R. T. Schwartz and H. S. Schwartz, Eds., Interscience Pub., New York, pp. 45-62, 1968.

16. J. Awerbuch and H. T. Hahn, unpublished results.

17. J. Haener, N. Ashbaugh, C. Y. Chia, and M. Y. Feng, "Investigation of Micromechanical Behavior of Fiber Reinforced Plastics," USAAVLABS-TR-66, AD-667901, 1968.

18. K. M. Prewo and K. G. Kreider, Failure Modes in Composites, The Metallurgical Society of the AIME, pp. 395-413, 1973.

19. H. T. Hahn, Journal of Composite Materials, Vol. 10, pp. 266-278, 1976.

20. H. T. Hahn and R. Y. Kim, "Swelling of Composite Laminates," presented at the ASTM Symposium on Environmental Effects on Advanced Composites, Dayton, Ohio, 1977. To be published in an ASTM STP.

21. G. D. Menke and I. J. Toth, Technical Report AFML-TR-71-102, Air Force Materials Laboratory, 1971.

22. M. J. Salkind and V. Patarini, Trans. AIME, Vol. 239, p. 1268, 1967.

23. J. R. Hancock, Technical Report AFFDL-TR-70-144, Air Force Flight Dynamics Laboratory, pp. 285-300, 1970.

24. G. D. Swanson and J. R. Hancock, Composite Materials: Testing and Design (Second Conference), ASTM STP 497, American Society for Testing and Materials, pp. 469-482, 1972.

25. J. R. Hancock, Composite Materials, Vol. 5, Fracture and Fatigue, L. J. Broutman, Ed., Academic Press, New York, pp. 371-414, 1974.

26. A. G. Metcalfe and M. J. Klein, Composite Materials, Vol. 1, Interfaces in Metal Matrix Composites, A. G. Metcalfe, Ed., Academic Press, New York, pp. 125-168, 1974.

27. G. J. Dvorak and J. Q. Tarn, Fatigue of Composite Materials, ASTM STP 569, American Society for Testing and Materials, pp. 145-168, 1975.

28. C.K.H. Dharan, Fatigue of Composite Materials, ASTM STP 569, American Society for Testing and Materials, pp. 171-188, 1975.

29. C.K.H. Dharan, Journal of Materials Science, Vol. 10, pp. 1665-1670, 1975.

REFERENCES (CONTINUED)

30. J. B. Sturgeon, Proc. of the 28th Annual Technical Conference, The Society of the Plastics Industry, Inc., 12-13, 1973.

31. J. B. Sturgeon, "Fatigue Testing of Carbon Fibre Reinforced Plastics," Technical Report 75135, Royal Aircraft Establishment, England, 1975.

32. M. J. Owen, Composite Materials, Vol. 5, Fracture and Fatigue, L. J. Broutman, Ed., Academic Press, New York, pp. 341-369, 1974.

33. J. Awerbuch and H. T. Hahn, Fatigue of Filamentary Composite Materials, ASTM STP, 636, pp. 248-266, 1977.

34. J. V. Mullin, V. F. Mazzio, and R. L. Mehan, NASA CR-121000 2420-N03, National Aeronautics and Space Administration, 1972.

35. B. W. Rosen, AIAA Journal, Vol. 2, pp. 1982-1991, 1964.

36. C. Zweben, AIAA Journal, Vol. 6, p. 2325, 1968.

37. J. C. Goan, T. W. Martin, and R. Prescott, Proc. of the 28th Technical Conference, The Society of Plastics Industry, Inc., 1973, 21-B.

38. Development of Engineering Data on the Mechanical and Physical Properties of Advanced Composite Materials, Technical Report AFML-TR-74-266, Air Force Materials Laboratory, 1975.

39. H. L. Hancox, Journal of Materials Science, Vol. 10, pp. 234-242, 1975.

40. I. J. Toth, W. D. Brentnall, and G. D. Menke, Journal of Metals, pp. 19-26, 37-42, 71-78, 1972.

41. R. C. Jones and J. L. Christian, Composite Materials: Testing and Design (Second Conference), ASTM STP 497, pp. 439-468, 1972.

42. Pipes, R. B., Composite Materials: Testing and Design (Third Conference), ASTM STP 546, pp. 419-432, 1972.

43. S. W. Tsai and H. T. Hahn, Composite Materials Workbook, Technical Report AFML-TR-77-33, Air Force Materials Laboratory, 1977.

44. D. F. Sims and V. H. Brogden, Fatigue of Filamentary Composite Materials, ASTM STP 636, American Society for Testing and Materials, pp. 185-205, 1977.

45. Z. Hashin and A. Rotem, Journal of Composite Materials, Vol. 7, pp. 448-464, 1973.

REFERENCES (CONTINUED)

46. A. Rotem, and Z. Hashin, AIAA Journal, Vol. 14, pp. 868-872, 1976.

47. H. T. Hahn, Journal of Composite Materials, Vol. 9, pp. 316-326, 1975.

48. R. B. Pipes and N. J. Pagano, Journal of Composite Materials, Vol. 4, pp. 538-548, 1970.

49. H. T. Hahn and S. W. Tsai, Journal of Composite Materials, Vol. 7, pp. 102-108, 1973.

50. H. T. Hahn, Journal of Composite Materials, Vol. 7, pp. 257-271, 1973.

51. R. S. Sandhu, Journal of Aircraft, Vol. 13, pp. 104-111, 1976.

52. S. W. Tsai and H. T. Hahn, Inelastic Behavior of Composite Materials, AMD-Vol. 13, C. T. Herakovich, Ed., American Society of Mechanical Engineers, pp. 73-96, 1975.

53. J. J. Nevadunsky, J. J. Lucas, and M. J. Salkind, Journal of Composite Materials, Vol. 9, pp. 394-408, 1975.

54. H. T. Hahn and R. Y. Kim, Journal of Composite Materials, Vol. 10, pp. 156-180, 1976.

55. L. J. Broutman and S. Sahu in Proc. of the 24th Technical Conference, The Society of Plastics Industry, 11-D, 1969.

56. F. J. McGarry, Fundamental Aspects of Fiber Reinforced Plastic Composites, R. T. Schwartz and H. S. Schwartz, Eds., Interscience Pub., New York, pp. 63-87, 1968.

57. M. J. Owen, Composite Materials, Vol. 5, Fracture and Fatigue, L. J. Broutman, Ed., Academic Press, New York, pp. 313-340, 1974.

58. T. Tanimoto and S. Amijima, Journal of Composite Materials, Vol. 9, pp. 380-390, 1975.

59. G. C. Grimes and P. H. Francis, Technical Report AFML-TR-75-33, Air Force Materials Laboratory, 1975.

60. H. T. Hahn, to be published.

61. K. L. Reifsnider, E. G. Henneke II, and W. W. Stinchcomb, Composite Materials: Testing and Design (Fourth Conference), ASTM STP 617, American Society for Testing and Materials, pp. 93-105, 1977.

62. J. W. Dally and L. J. Broutman, Journal of Composite Materials, Vol. 1, pp. 424-442, 1967.

REFERENCES (CONTINUED)

63. G. P. Sendeckyj and H. D. Stalnaker, Composite Materials; Testing and Design (Fourth Conference), ASTM STP 617, American Society for Testing and Materials, pp. 39-52, 1977.

64. B. E. Kaminski, G. H. Lemon, and E. L. McKague, Technical Report AFML-TR-70-108, Vol. 1, Air Force Materials Laboratory, 1972.

65. S. V. Ramani and D. P. Williams, Fatigue of Filamentary Composite Materials, ASTM STP 636, American Society for Testing and Materials, pp. 27-46, 1977.

66. J. T. Ryder and E. K. Walker, Ascertainment of the Effect of Compressive Loading on the Fatigue Lifetime of Graphite Epoxy Laminates for Structural Applications, Technical Report AFML-TR-76-241, Air Force Materials Laboratory, 1976.

67. F. H. Chang, D. E. Gordon, B. T. Rodini, and R. H. McDaniel, Journal of Composite Materials, Vol. 10, pp. 182-192, 1976.

68. F. H. Chang, D. E. Gordon, and A. H. Gardner, Fatigue of Filamentary Composite Materials, ASTM STP 636, American Society for Testing and Materials, pp. 57-72, 1977.

69. J. H. Underwood and D. P. Kendall, Proc. of the 1975 International Conference on Composite Materials, Vol. 2, The Metallurgical Society of the AIME, pp. 1122-1132, 1976.

70. E. Durchlaub and P. Sacco, Technical Report AFFDL-TR-72-82, Air Force Flight Dynamics Laboratory, 1972.

71. K. L. Reifsnider, W. W. Stinchcomb, and T. K. O'Brien, Fatigue of Filamentary Composite Materials, ASTM STP 636, American Society for Testing and Materials, pp. 171-184, 1977.

72. M. S. Rosenfeld and S. L. Huang, presented at the AIAA/ASME Structures, Dynamics and Materials Conference, San Diego, 1977.

73. L. G. Bevan, Composites, Vol. 8, pp. 227-232, 1977.

74. L. A. Marcus and W. W. Stinchcomb, Experimental Mechanics, Vol. 15, pp. 55-60, 1975.

75. M. J. Owen, J. R. Griffiths, and M. S. Found, Proc. of the 1975 International Conference on Composite Materials, The Metallurgical Society of the AIME, pp. 917-941, 1976.

76. P. H. Francis, D. E. Walrath, D. F. Sims, and D. N. Weed, Journal of Composite Materials, Vol. 11, pp. 488-501, 1977.

77. D. C. Phillips and J. M. Scott, Composites, Vol. 8, pp. 233-236, 1977.

REFERENCES (CONCLUDED)

78. H. T. Sumsion and D. P. Williams, Fatigue of Composite Materials, ASTM STP 569, American Society for Testing and Materials, pp. 226-247, 1975.

79. M. J. Owen and S. Morris, Proc. of the 25th Annual Technical Conference, The Society of Plastics Industry, 8-E, 1970.

80. D. K. Lloyd and M. Lipow, Reliability: Management, Methods, and Mathematics, Prentice Hall, Englewood Cliffs, New Jersey, 1962.

81. B. D. Coleman, Journal of Applied Physics, Vol. 29, pp. 968-983, 1958.

82. S. L. Phoenix, "Stochastic Strength and Fatigue of Fiber Bundles," Report under NSF Grant ENG 75-00570, Cornell University.

83. J. C. Halpin, K. L. Jerina, and T. A. Johnson, The Test Methods for High Modulus Fibers and Composites, ASTM STP 521, American Society for Testing and Materials, pp. 5-64, 1973.

84. H. T. Hahn and R. Y. Kim, Journal of Composite Materials, Vol. 9, pp. 297-311, 1975.

85. R. P. Haviland, Engineering Reliability and Long Life Design, D. Van Nostrand Co., Princeton, New Jersey, 1964.

86. J. N. Yang, Journal of Composite Materials, Vol. 11, pp. 193-203, 1977.

87. J. N. Yang, Mechanics of Composites Review, Air Force Materials Laboratory, Air Force Office of Scientific Research, Air Force Flight Dynamics Laboratory, pp. 51-60, 1977.

88. L. J. Broutman and S. Sahu, Composite Materials: Testing and Design (Second Conference), ASTM STP 497, American Society for Testing and Materials, pp. 170-188, 1972.

TABLE 1

FATIGUE FAILURE FUNCTIONS

Max. Stress Theory [43]	$\text{Max}\left\{\sigma_1/S_L,\ \sigma_2/S_T,\ \sigma_6/S_S\right\} = 1$
	$S_\alpha = a_\alpha - b_\alpha \log N$
Tsai-Hill Theory [44]	$\frac{\sigma_1^2}{S_L^2} - \frac{\sigma_1\sigma_2}{S_L^2} + \frac{\sigma_2^2}{S_T^2} + \frac{\sigma_6^2}{S_S^2} = 1$
	$S_\alpha = a_\alpha + b_\alpha/N^x - c_\alpha/A^y$
Hashin [45,46]	$\text{Max}\left\{\frac{\sigma_1}{S_L},\ \left(\frac{\sigma_2^2}{S_T^2} + \frac{\sigma_6^2}{S_S^2}\right)\right\} = 1$
	$S_\alpha = a_\alpha - b_\alpha \log N$

Remarks

(1) a_α, b_α, and c_α are material constants

(2) $A = S_a/S_m = (1-R)/(1+R)$: S_a = alternating stress; S_m = mean stress.

(3) The same procedure is repeated the sign changes in each stress component.

TABLE 2

FATIGUE PARAMETERS

Material	R	α	β	γ	Reference
(0) Gr/Ep	1	0.30	78	79.7[(a)]	82
(0) Kevlar 49/Ep	1	0.87	42	57.2[(a)]	
(0) S-Gl/Ep	1	0.75	30	44.8[(a)]	
(0) Be/Ep	1	3.75	26	73.8[(a)]	
(0/±45/90) E-Gl/Ep	1	1.00	12.46	11.58	83
(0/±45/90) E-Gl/Ep	0.1	1.36	12.92	8.25	83
$[0/90/\pm45]_s$ Gr/Ep	0.1	1.37	17.78	9.82	86
(0/±45/90) Gr/Ep	0	2.06	17.34	11.13	87
(0/±45/90) Gr/Ep	S_{min} = -110 MPa	2.08	12.27	11.0	87

(a) α_s was estimated from the coefficient of variation (CV) by $\alpha_s = (1/CV)^{1.0638}$.

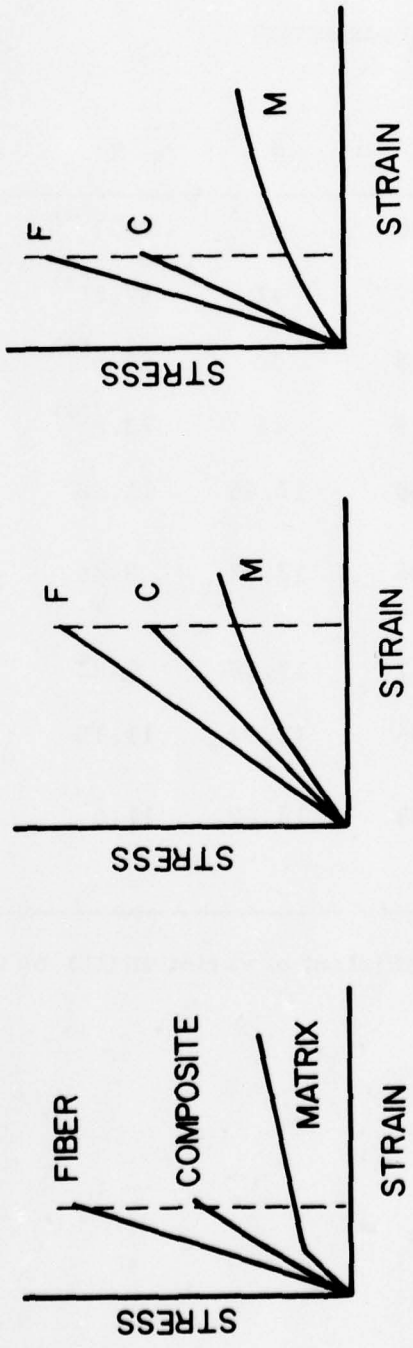

Figure 1. Schematic Stress-Strain Curves of Composites and Constituents: (a) Metal Matrix Composites; (b) Glass Fiber Reinforced Plastics; (c) Advanced Polymer Matrix Composites

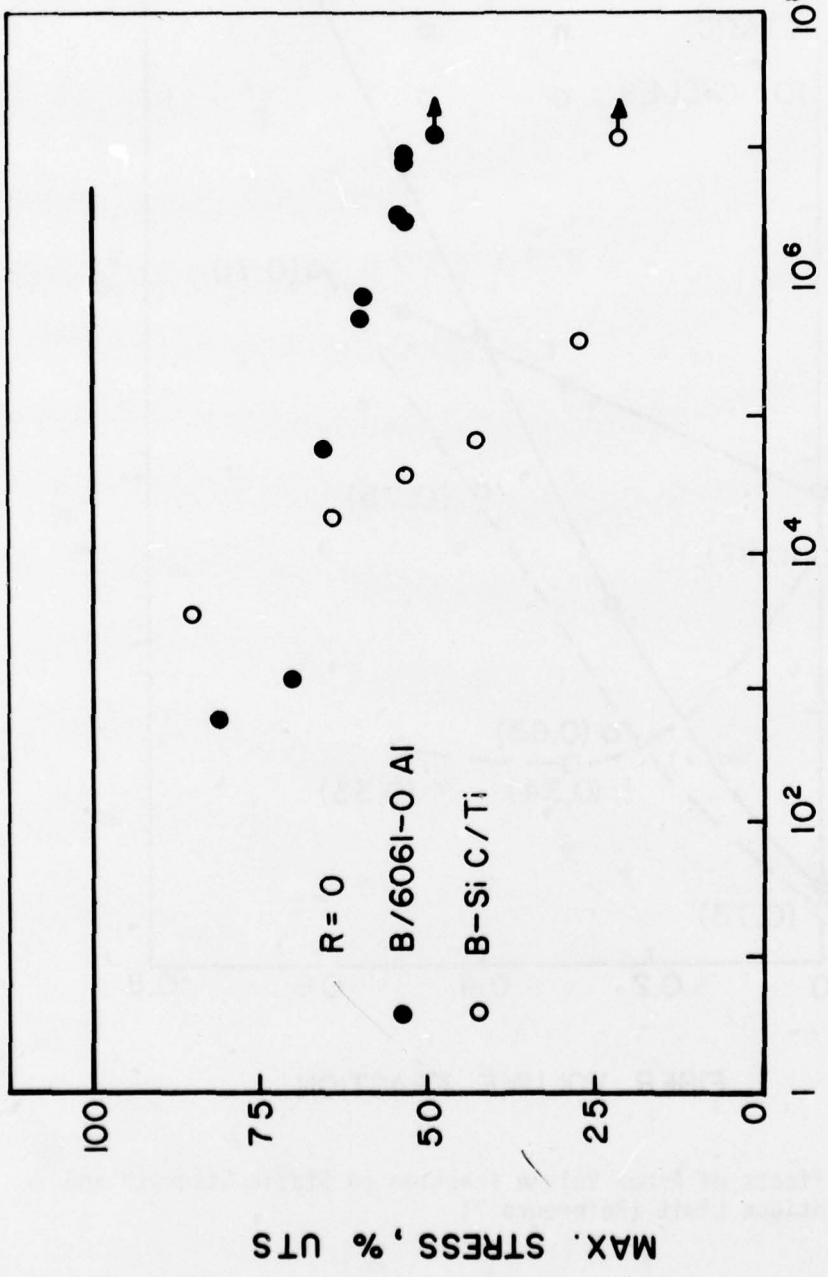

Figure 2. Longitudinal S-N Data, B/Al and BSiC/Ti (UTS=1698 MPa for B/Al and 1296 MPa for BSiC/Ti) (References 7, 9)

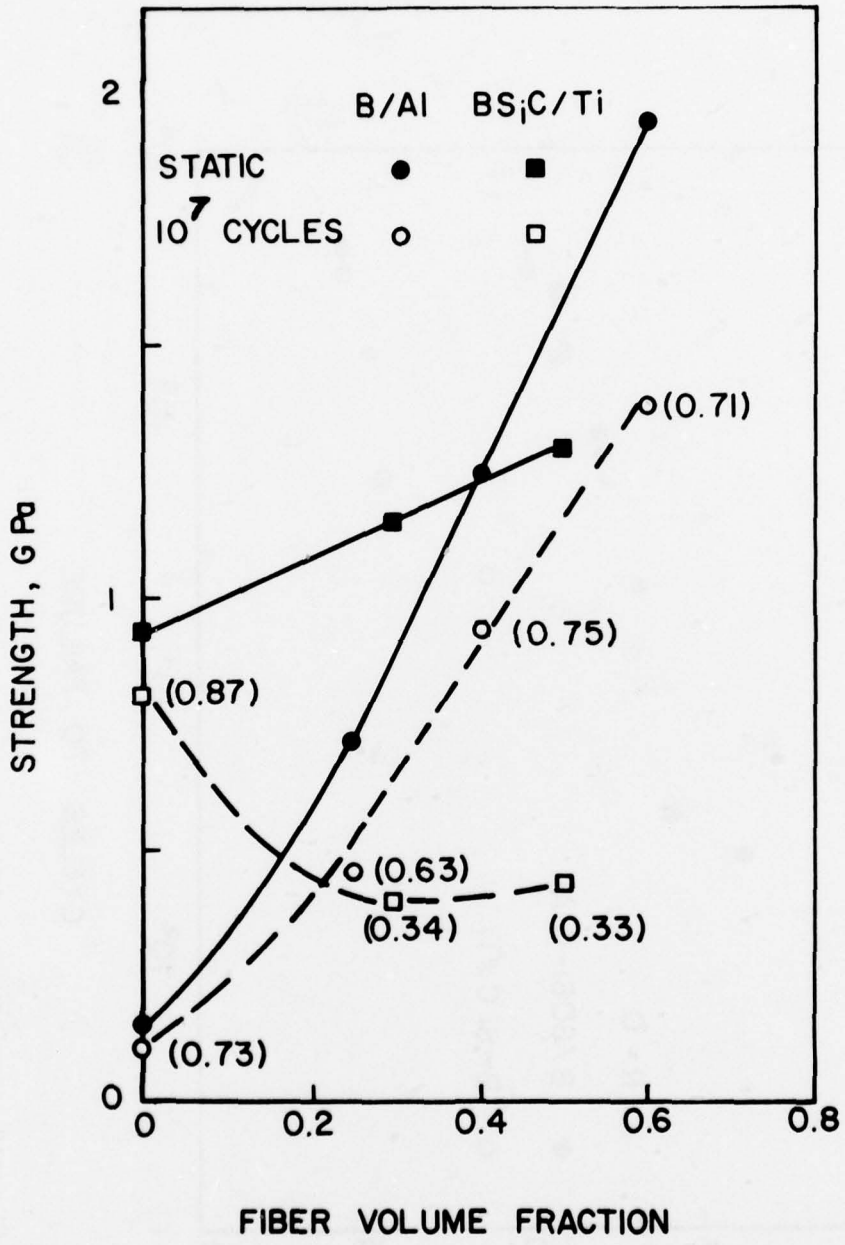

Figure 3. Effects of Fiber Volume Fraction on Static Strength and Fatigue Limit (Reference 7)

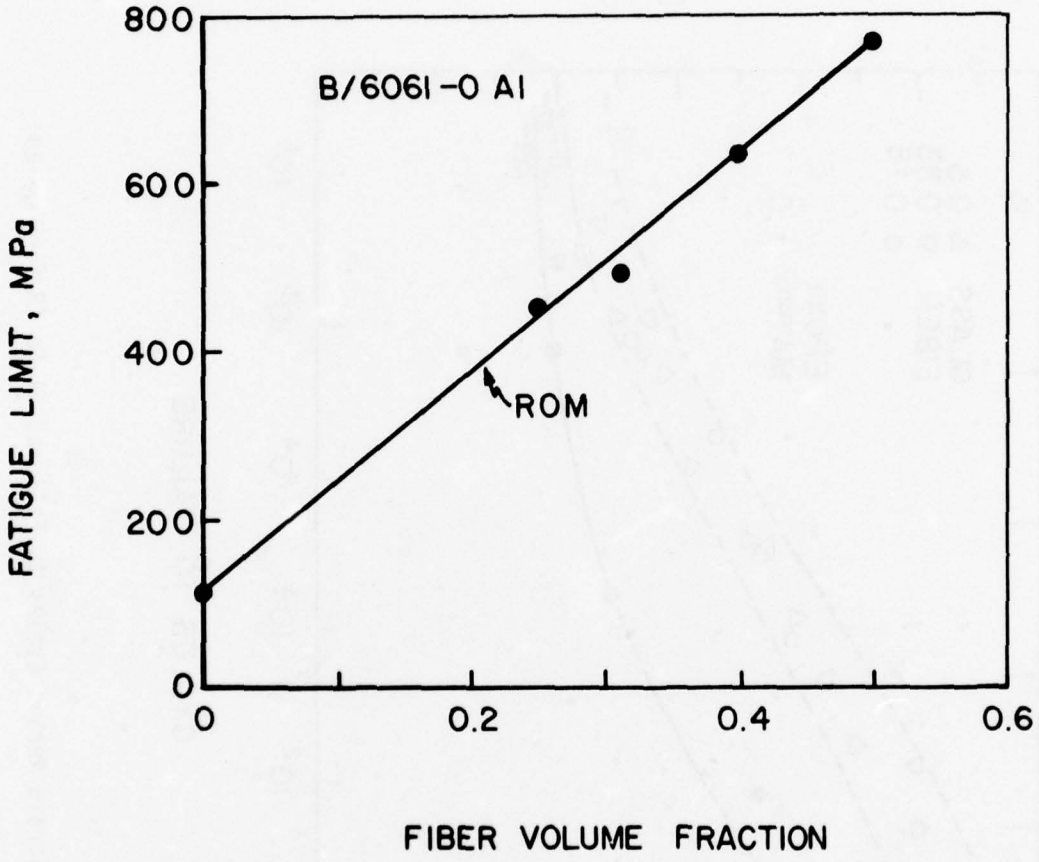

Figure 4. Fatigue Limit Predicted by Rule of Mixtures (Reference 25)

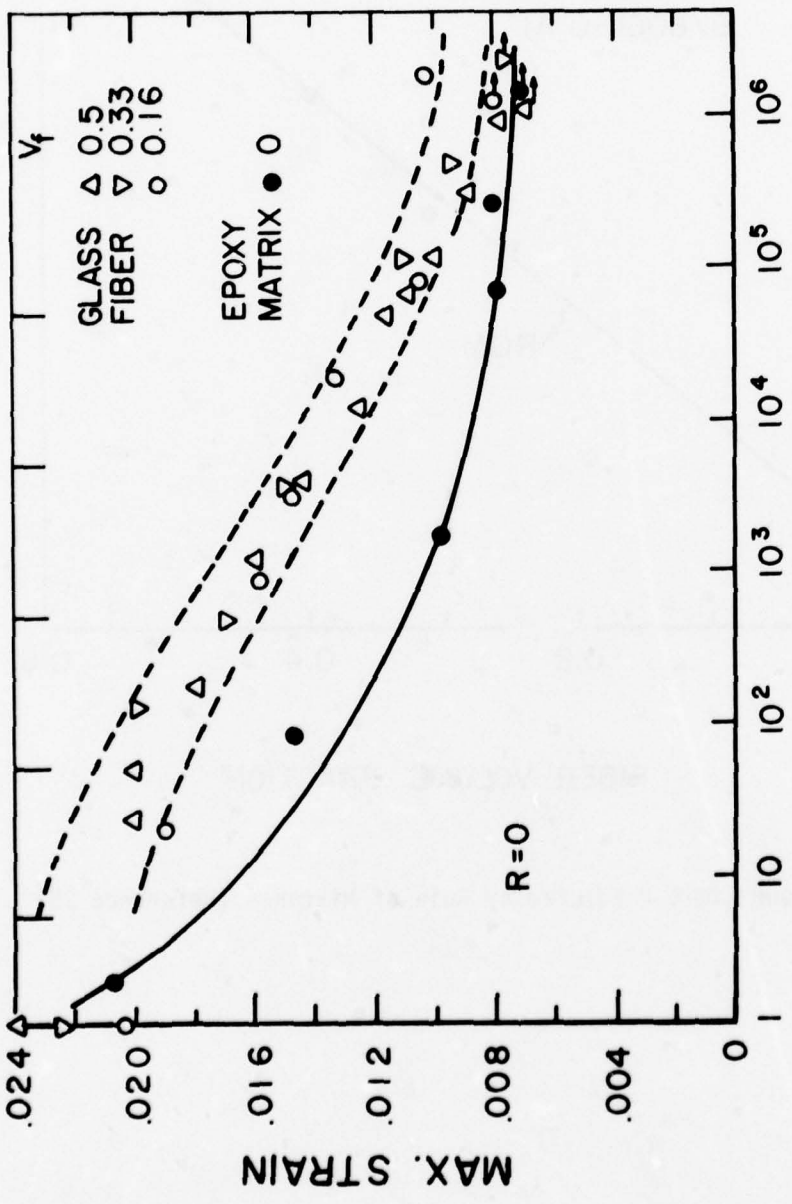

Figure 5. Maximum Strain versus Cycles to Failure, Gl/Ep (Reference 29)

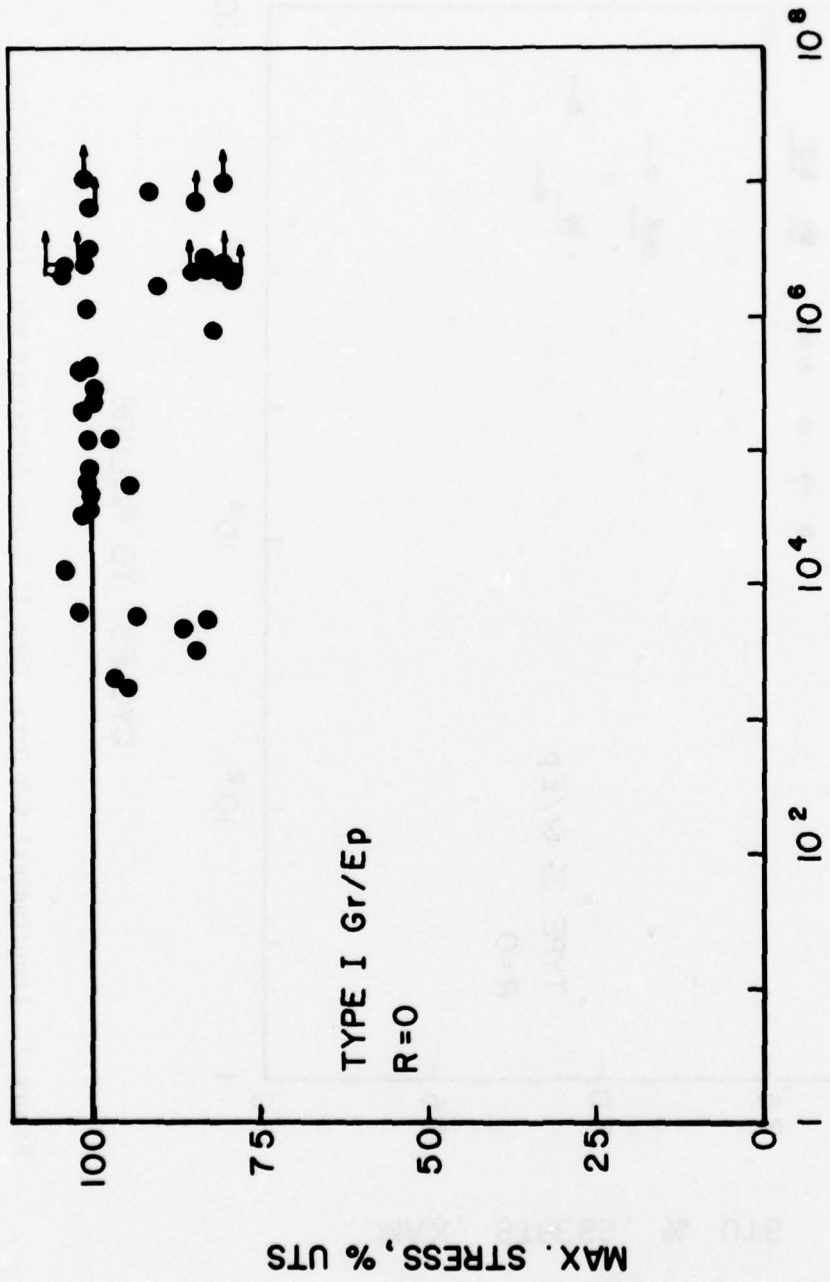

Figure 6. Longitudinal S-N Data, Type I Gr/Ep (UTS=872 MPa) (Reference 30)

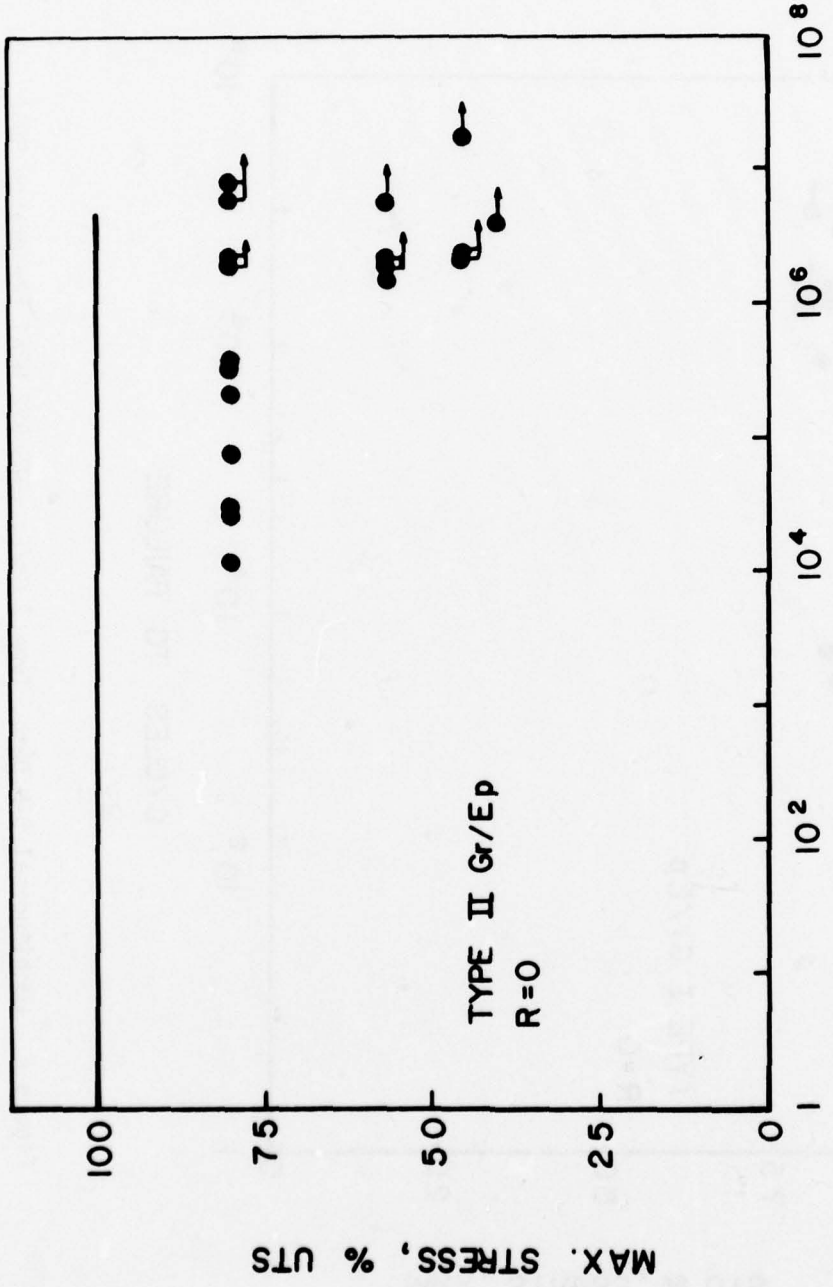

Figure 7. Longitudinal S-N Data, Type II Gr/Ep (UTS=1345 MPa) (Reference 31)

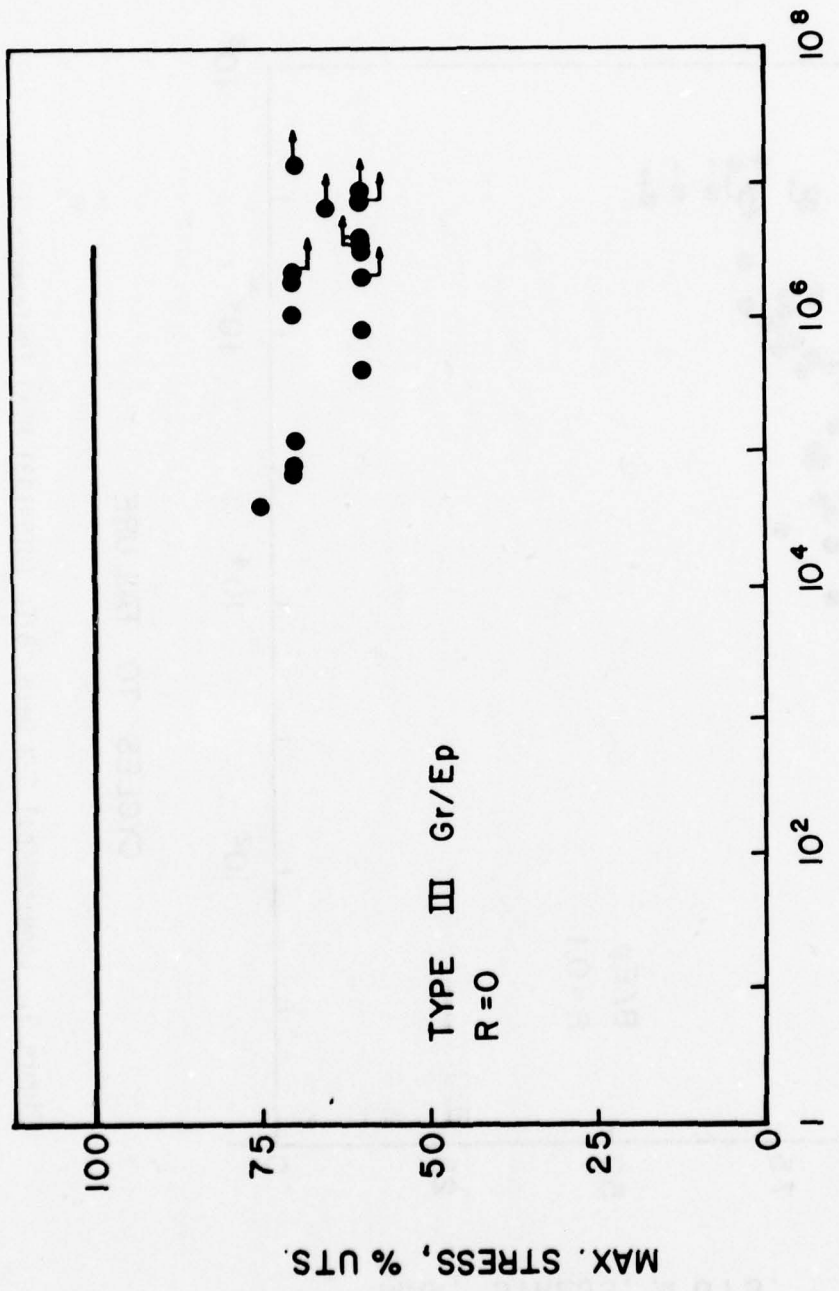

Figure 8. Longitudinal S-N Data, Type III Gr/Ep (UTS=1732 MPa) (Reference 31)

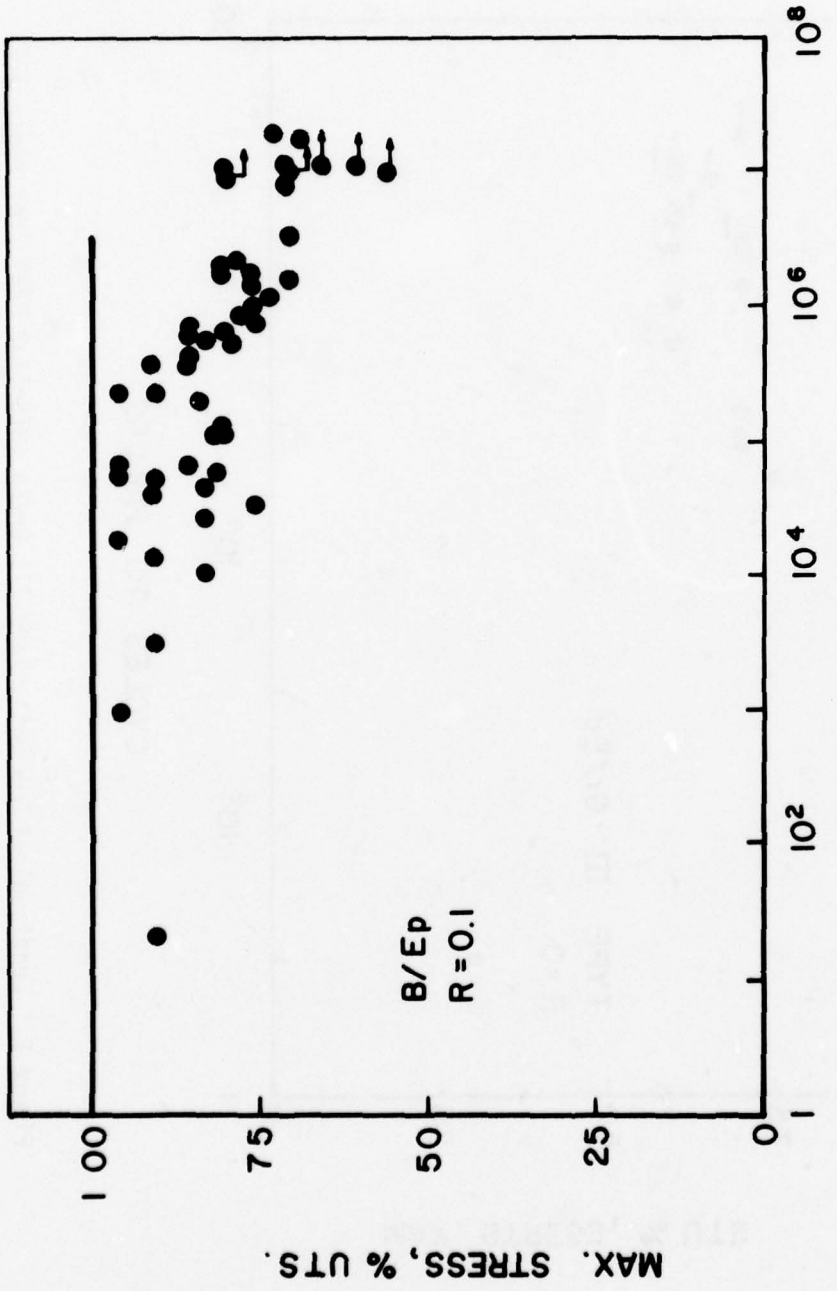

Figure 9. Longitudinal S-N Data, B/Ep (UTS=1331 MPa) (Reference 3)

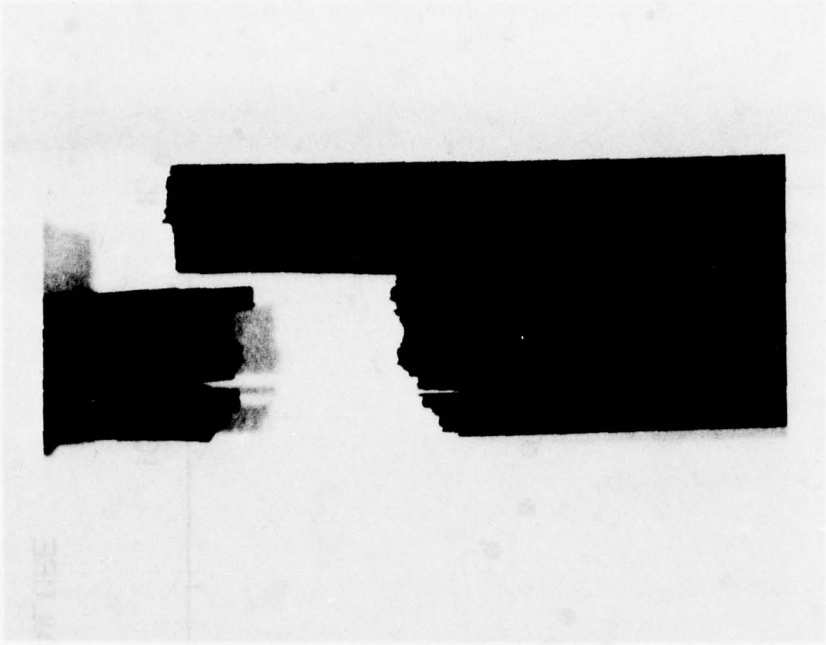

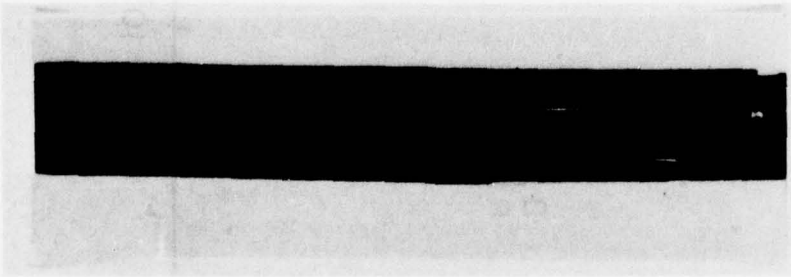

Figure 10. Typical Failure Modes of Gr/Ep: (a) Strong Interphase (b) Weak Interphase

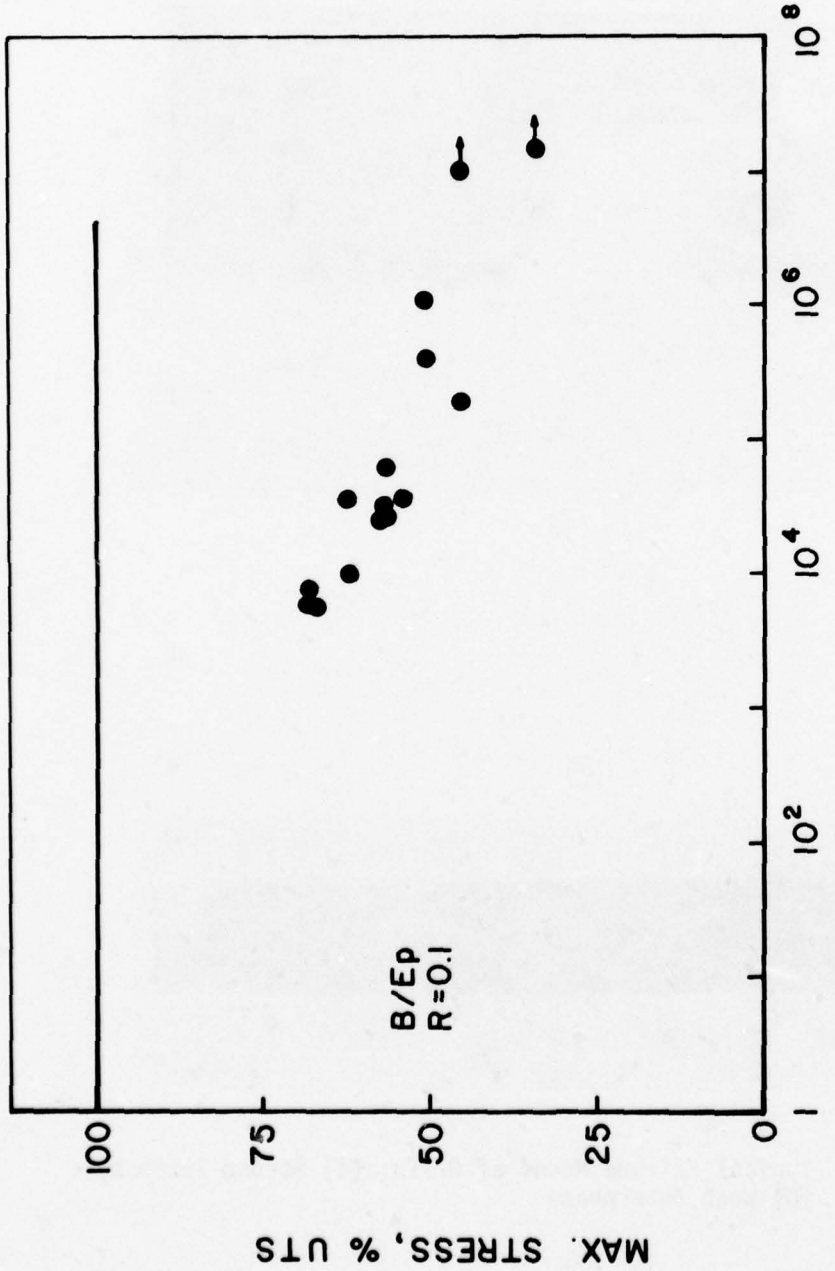

Figure 11. Transverse S-N Data, B/Ep (UTS=60.9 MPa) (Reference 3)

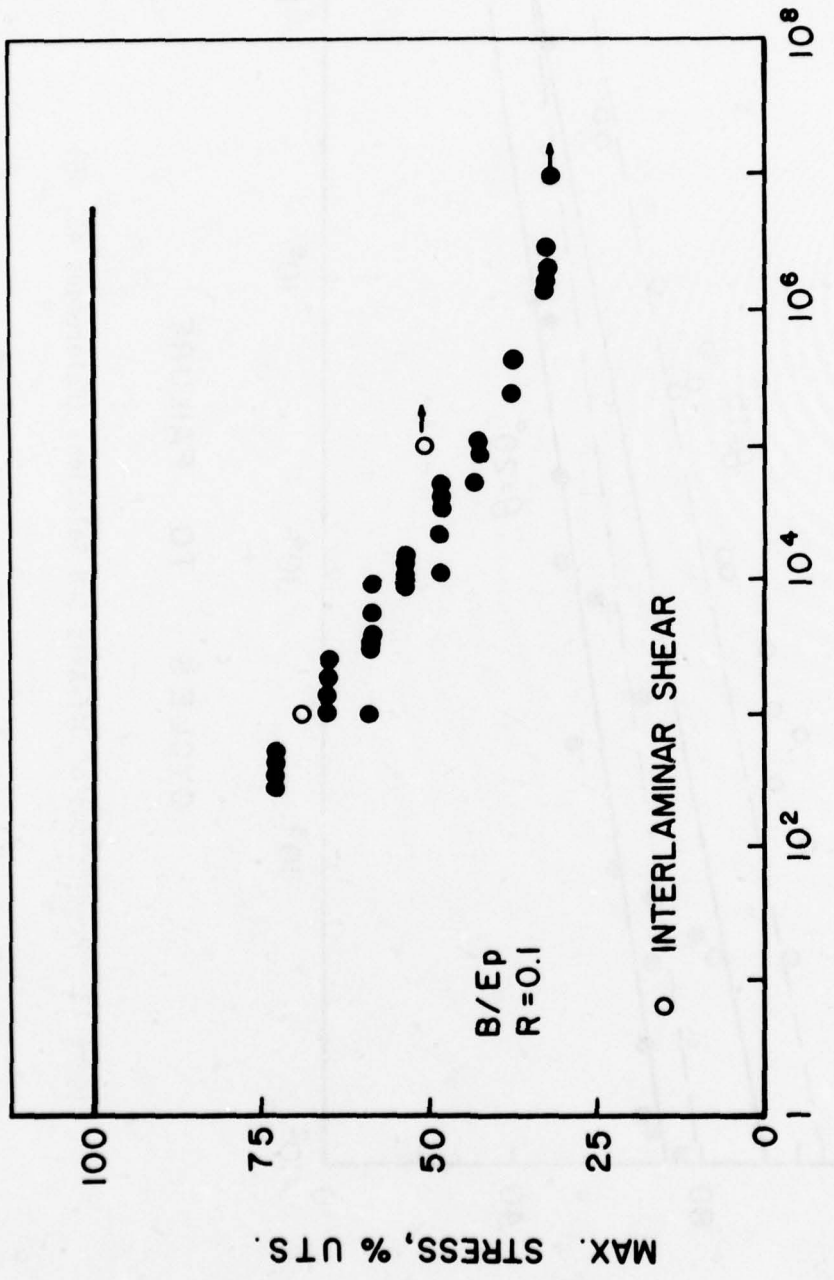

Figure 12. Shear S-N Data, B/Ep (Longitudinal Shear Strength = 66.7 MPa, Interlaminar Shear Strength = 81.4 MPa) (References 3, 5, 42)

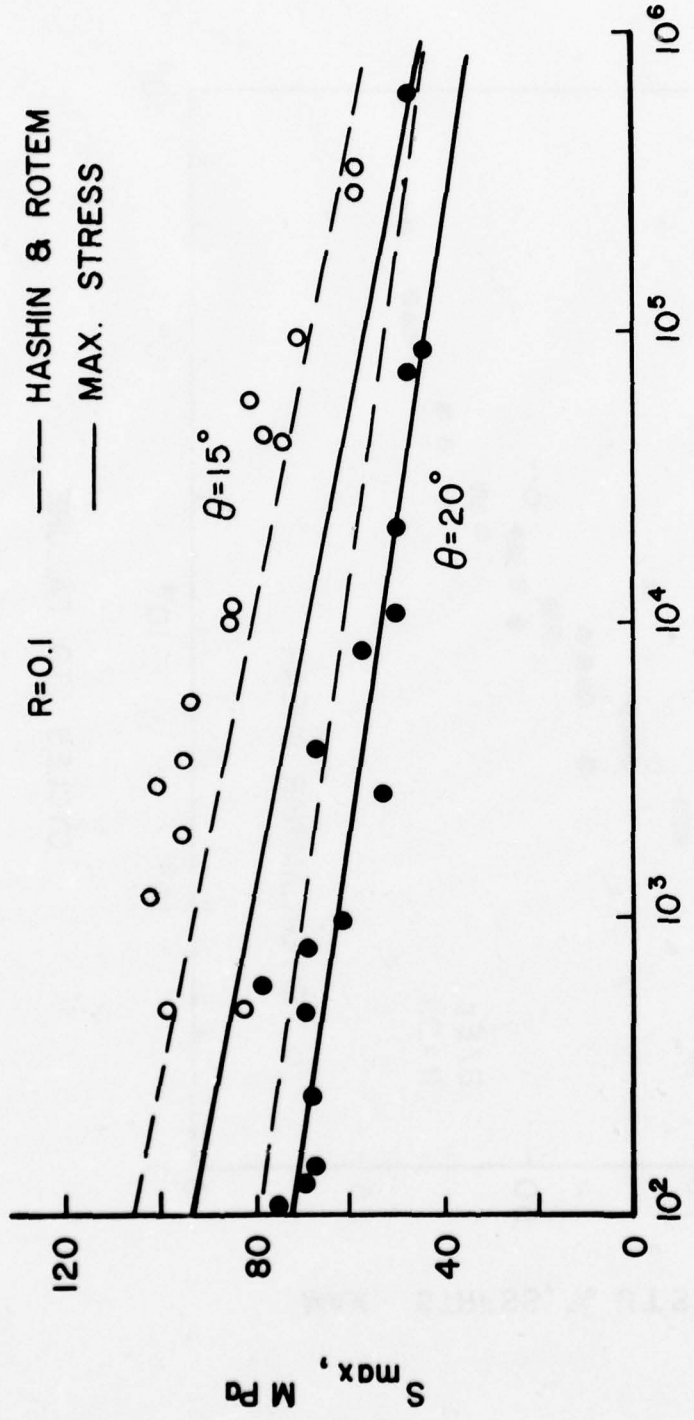

Figure 13. Predictions of Off-Axis S-N Relations (References 43, 45)

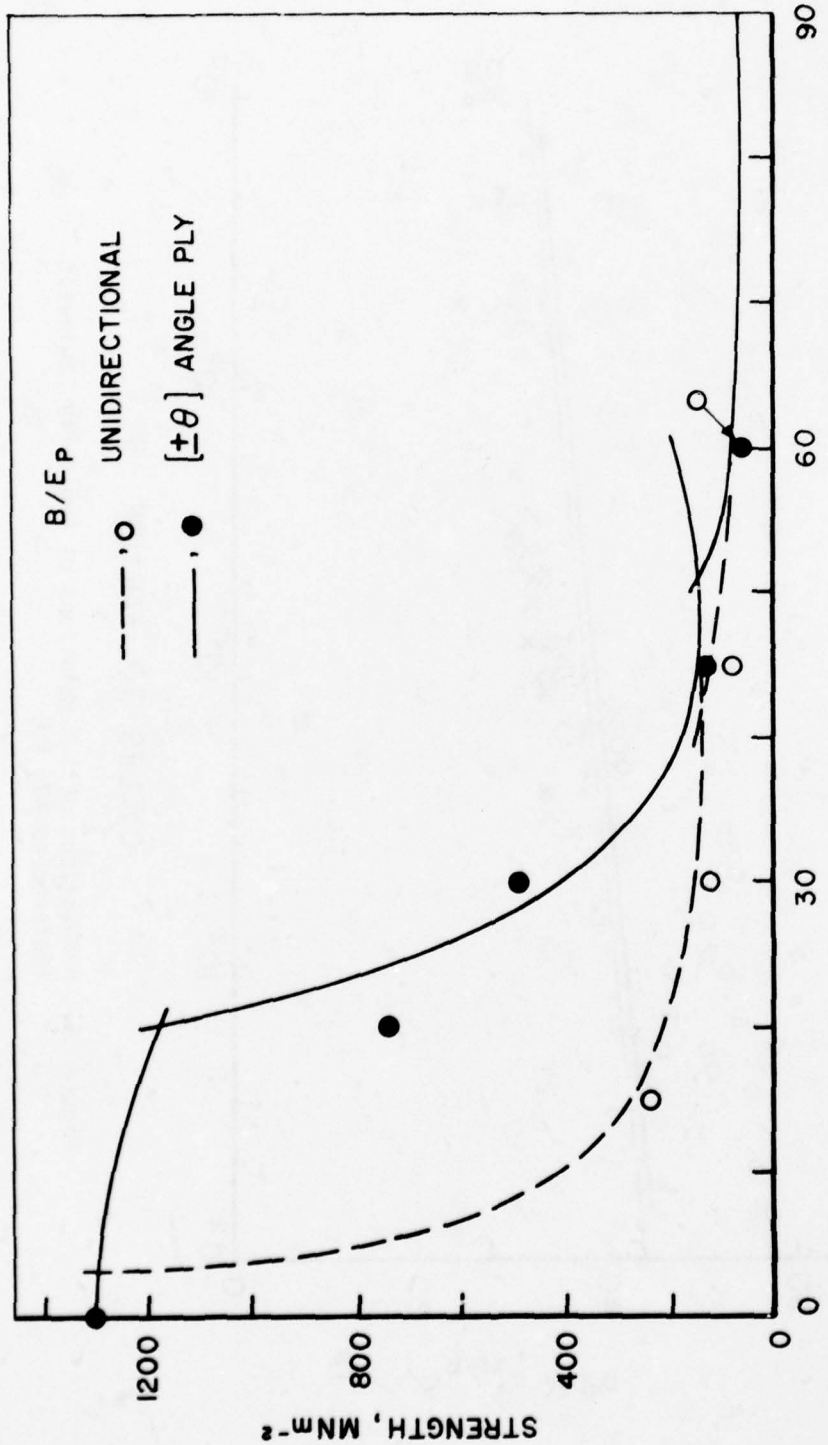

Figure 14. Comparison Between Strengths of Angle-Ply Laminates and Off-Axis Strength (Reference 47)

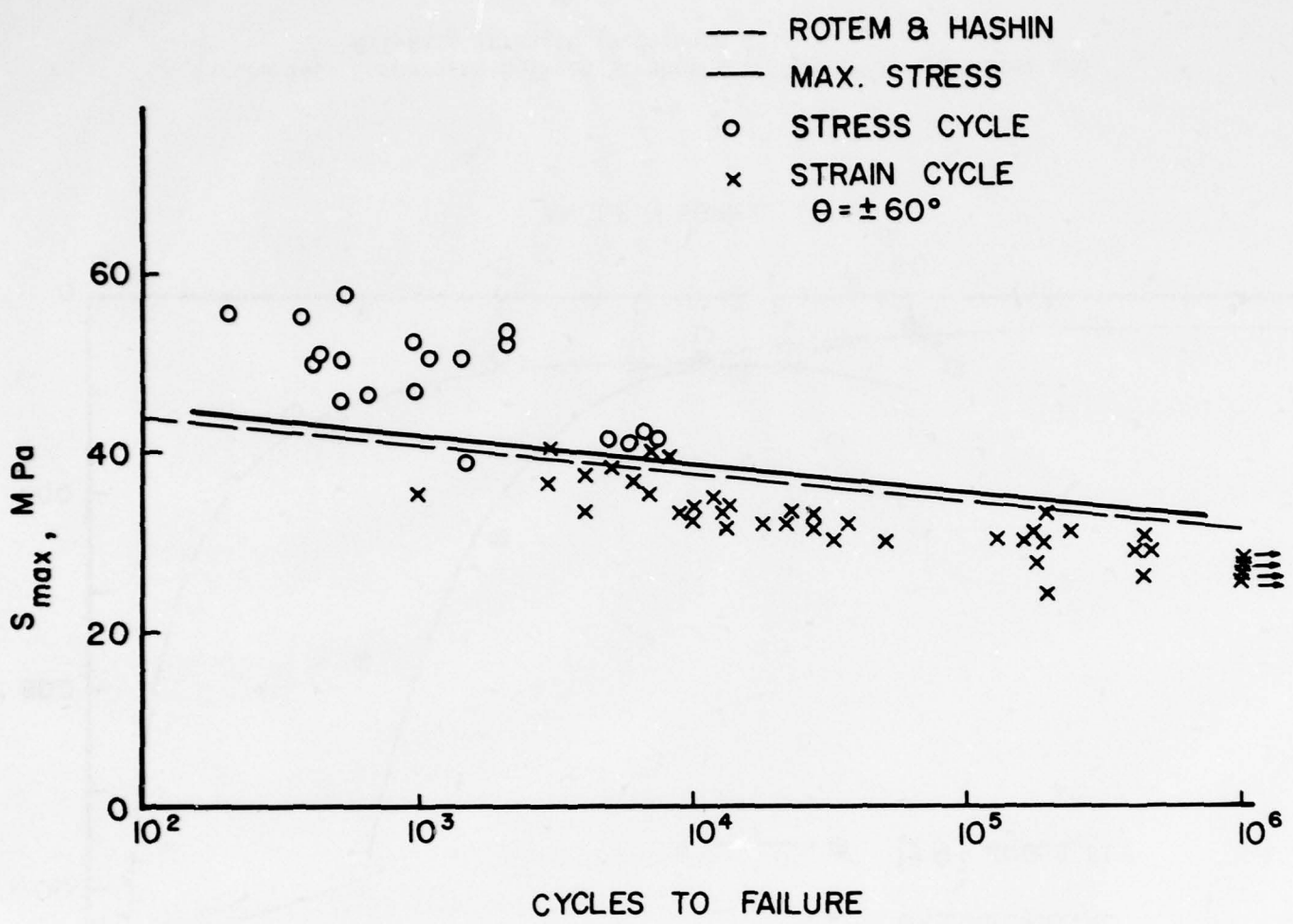

Figure 15. Predictions of S-N Relations of Angle-Ply Laminates (References 43, 46)

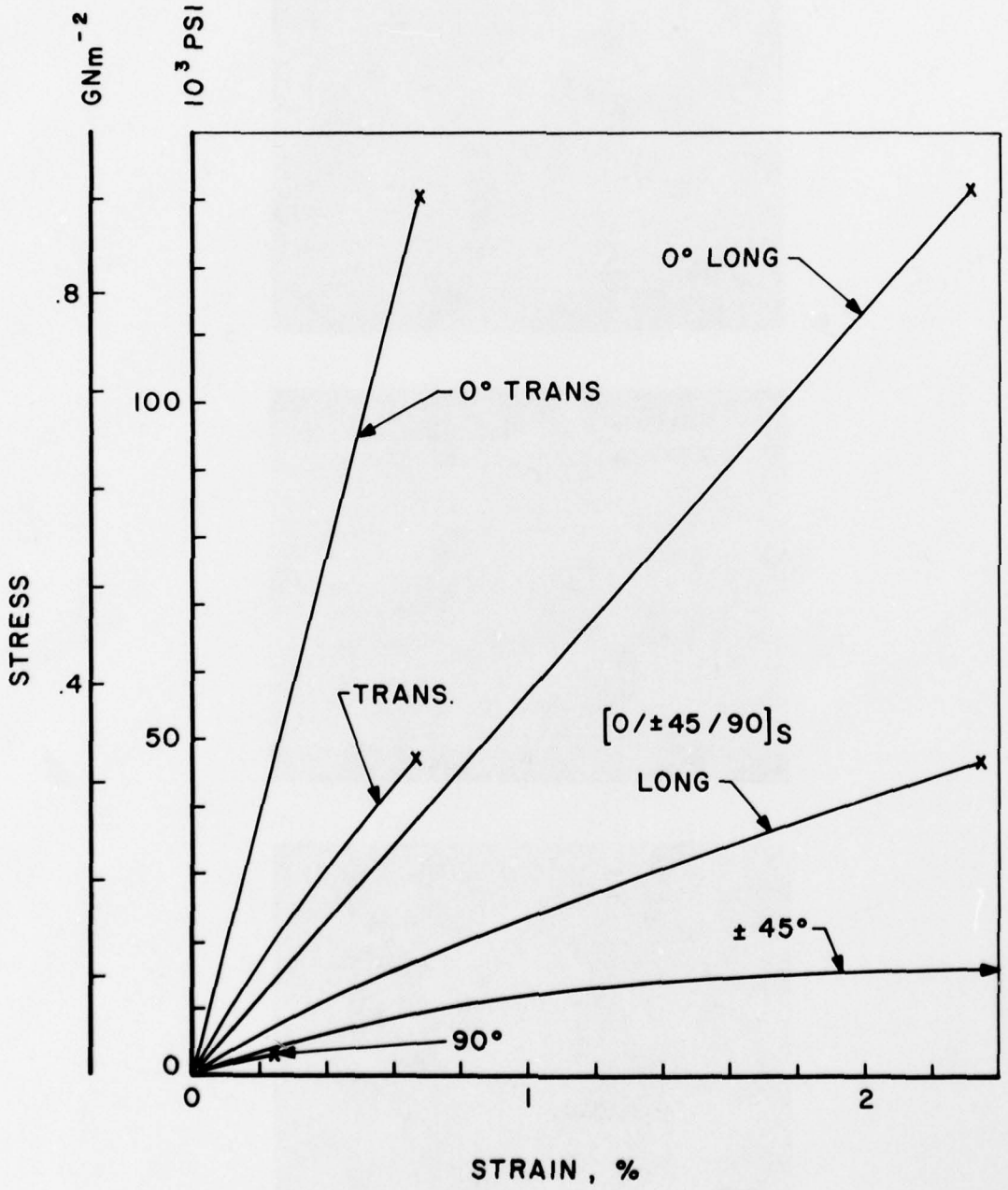

Figure 16. Stress-Strain Relations of $(0/\pm 45/90)_s$ Gl/Ep and of Constituent Plies (Reference 54)

Figure 17. Failure Modes at Free Edge: (a) $(0/90)_s$; (b) $(0/\pm45)_s$; (c) $(0/\pm45/90)_s$

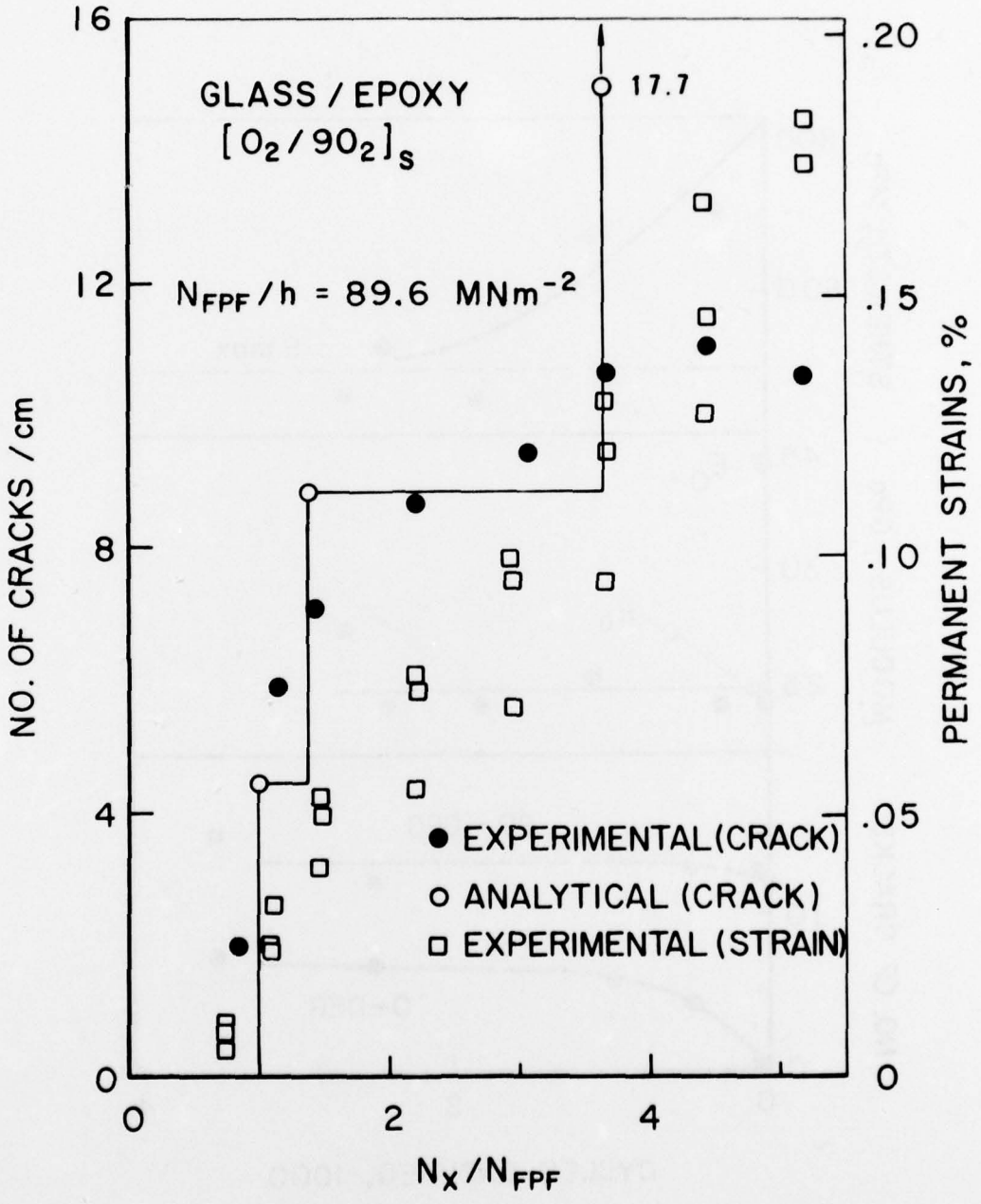

Figure 18. Number of Transverse Cracks Versus Laminate Stress (Reference 52)

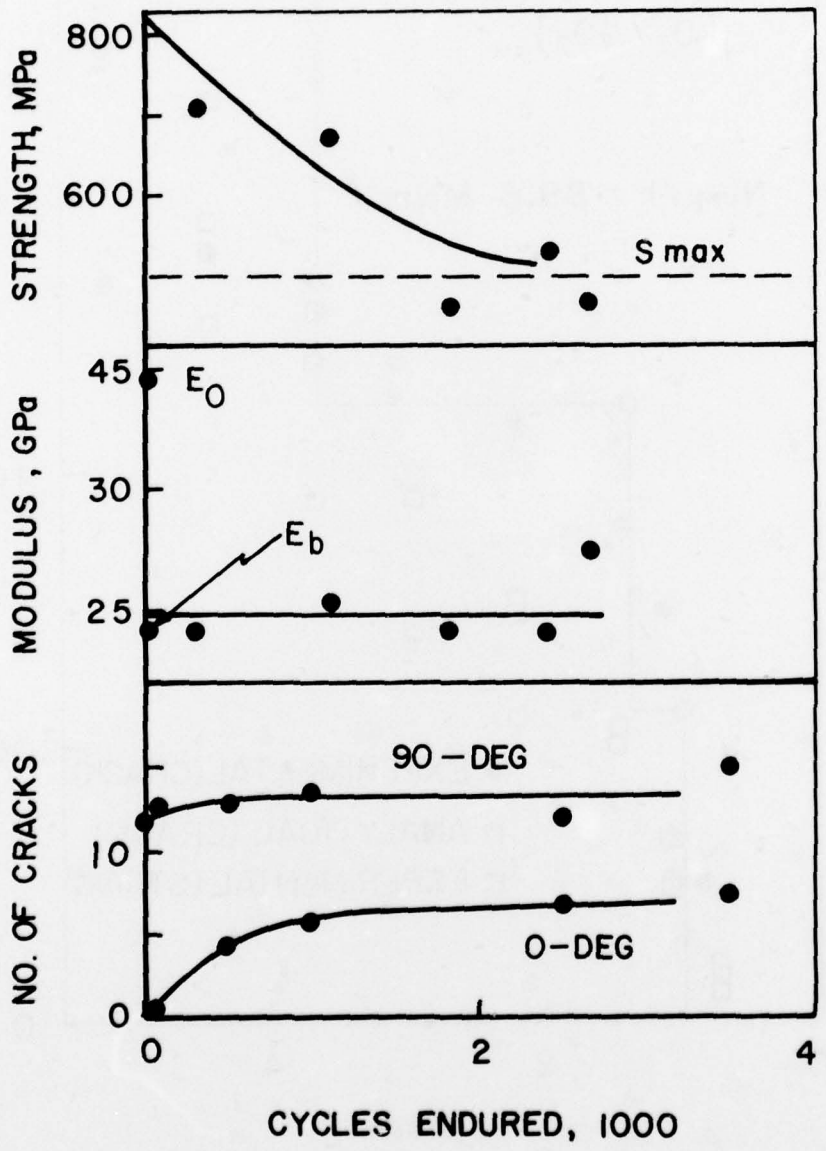

Figure 19. Damage Indications in Cross-Ply Gl/Ep Laminate (Reference 55)

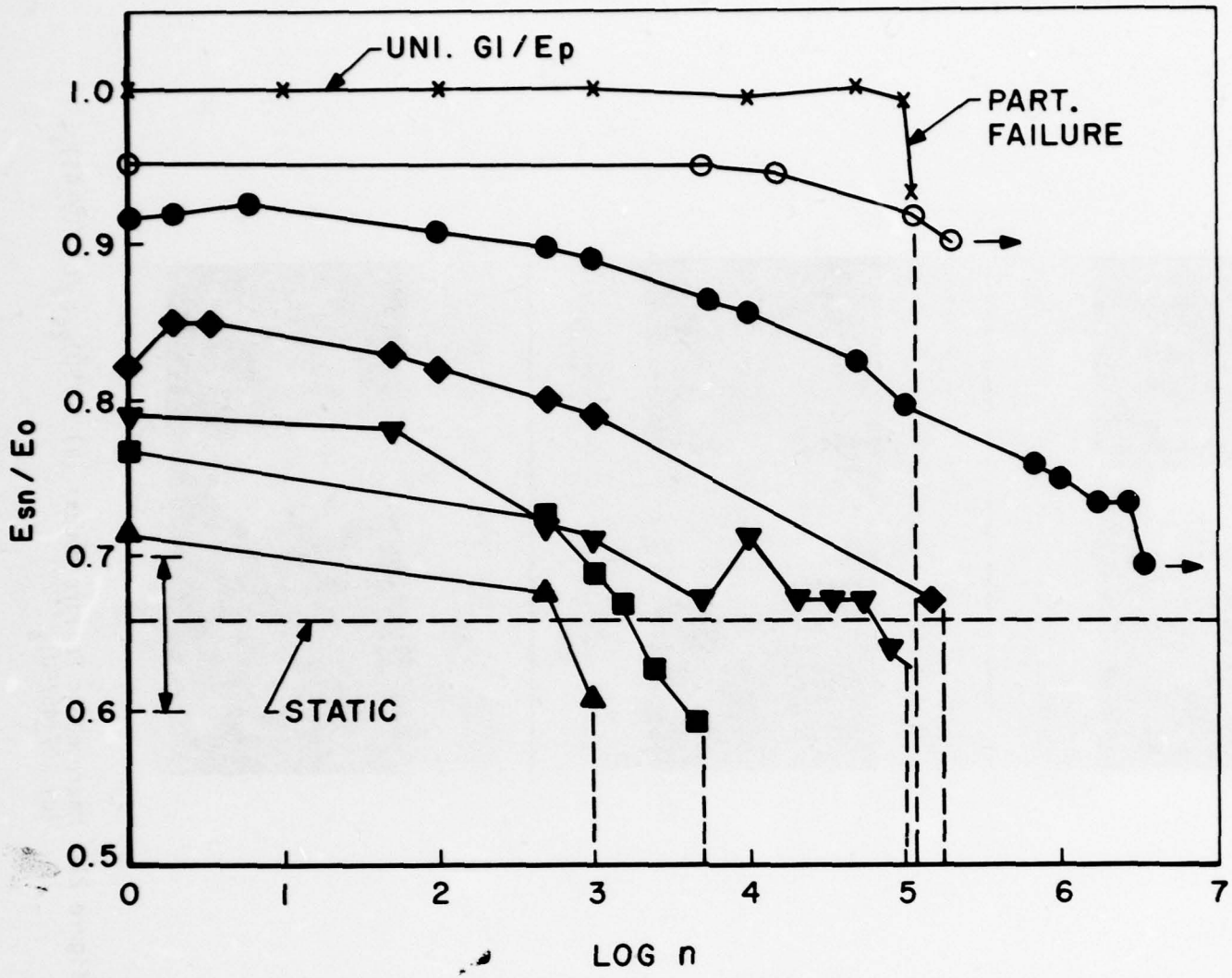

Figure 20. Change of Secant Modulus in Fatigue of $(0/\pm45/90)_S$ Gl/EP (Reference 54)
S_{max} = 62 (o), 103 (●), 138 (◆), 172 (▼), 207 (■), 248 MPa (▲)

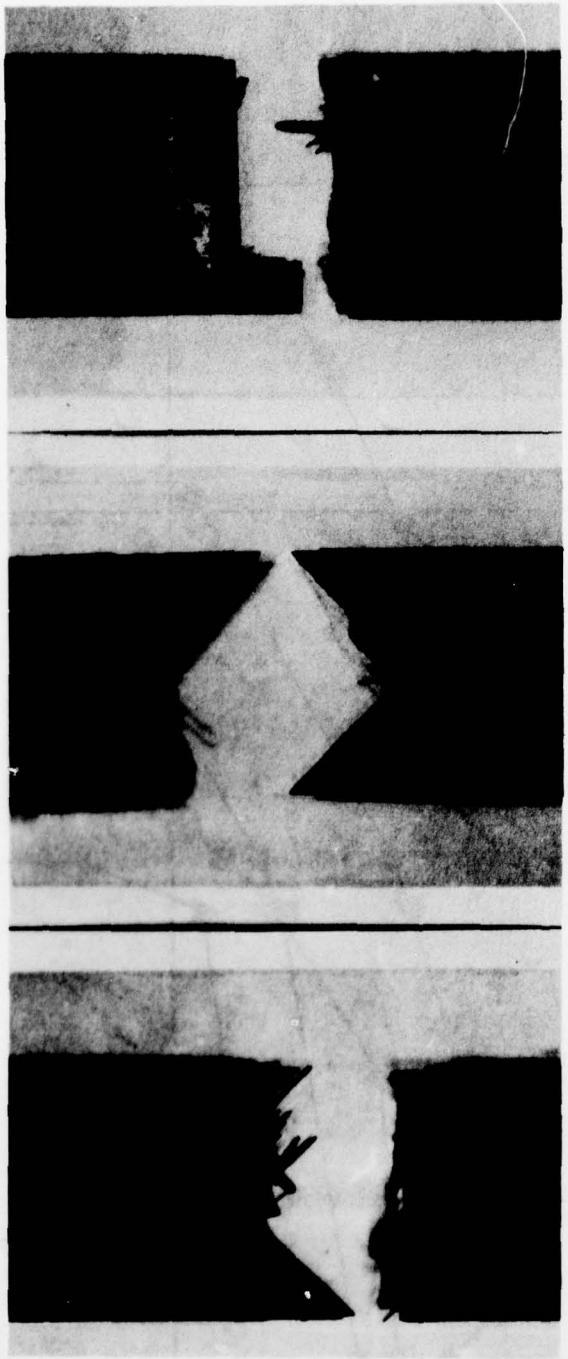

Figure 21. Macroscopic Failure Modes: (a) $(0/90)_{2s}$; (b) $(0/\pm45)_s$; (c) $(0/\pm45/90)_s$

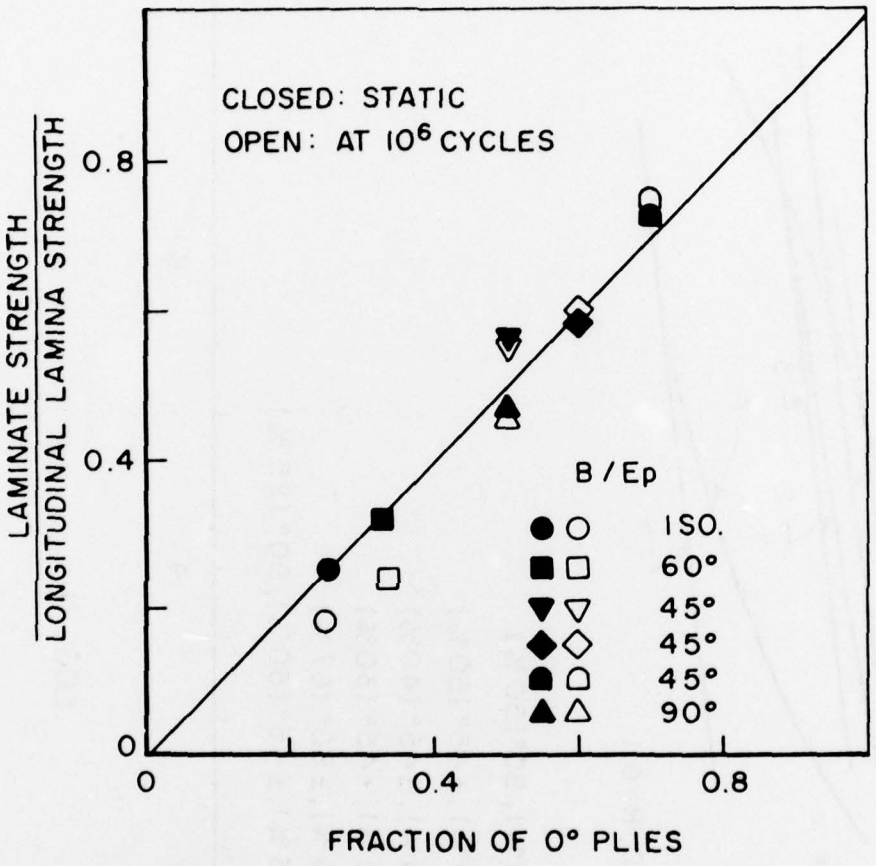

Figure 22. Static and Fatigue Strengths of Fiber-Controlled Laminates (Data from Reference 3)

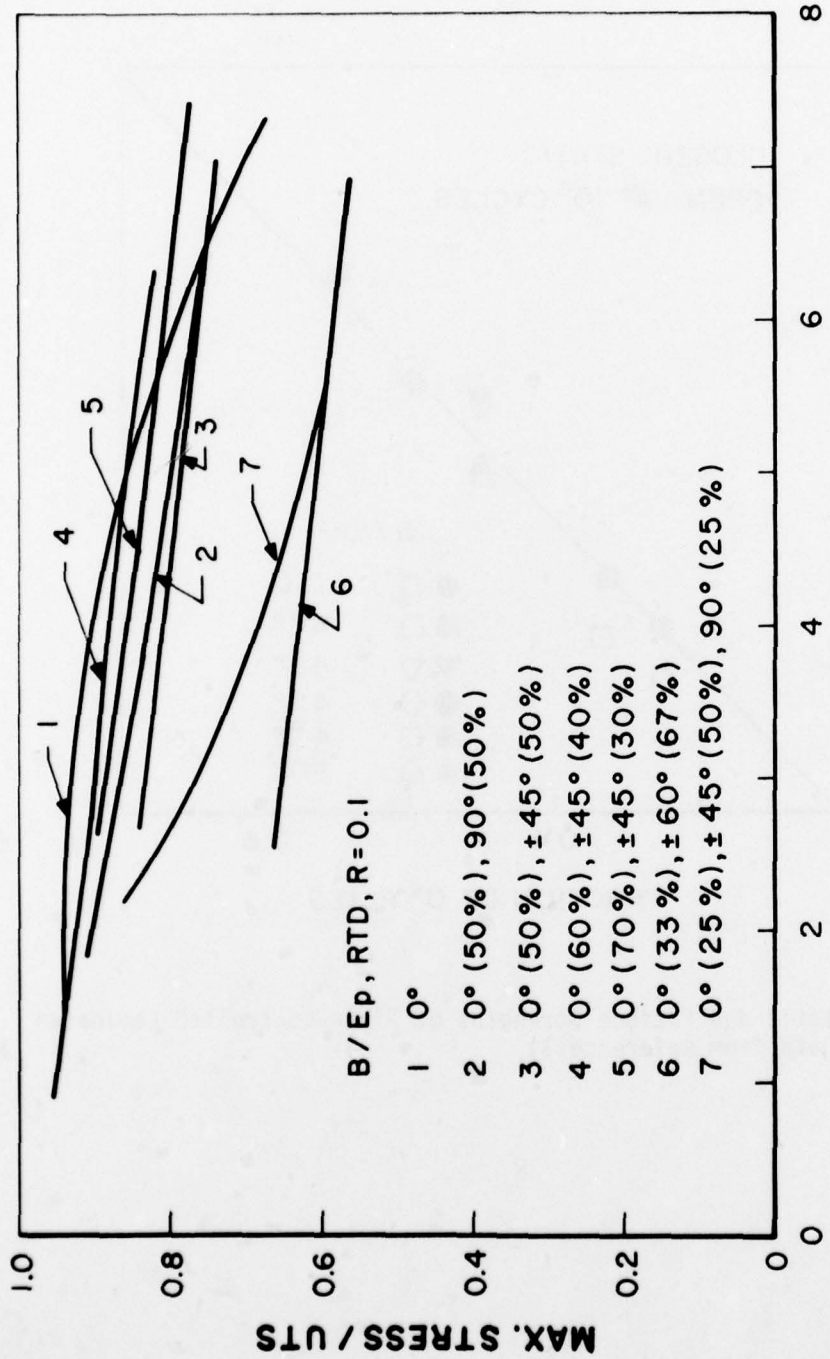

Figure 23. Normalized S-N Curves of Fiber-Controlled Laminates (Reference 3)

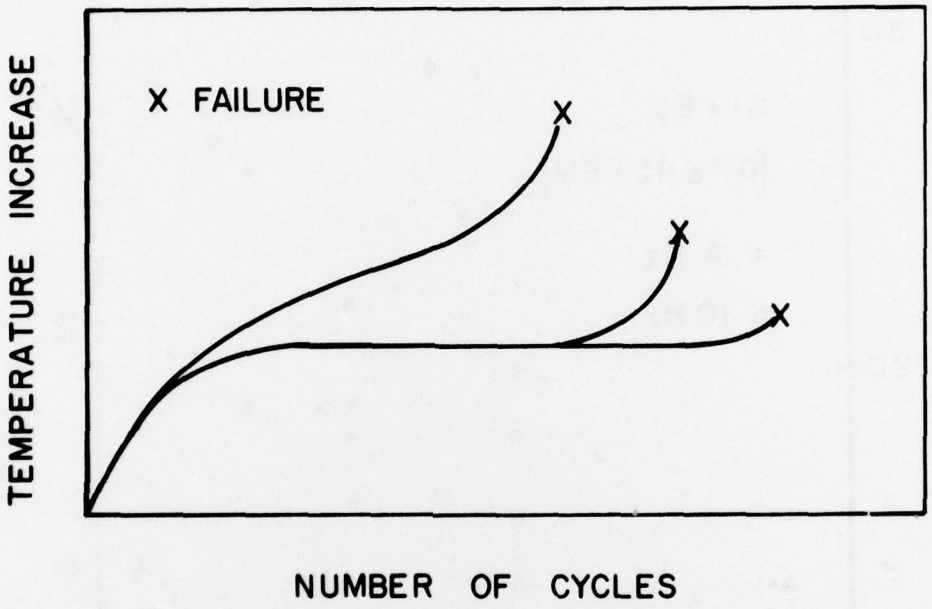

Figure 24. Typical Temperature Increase

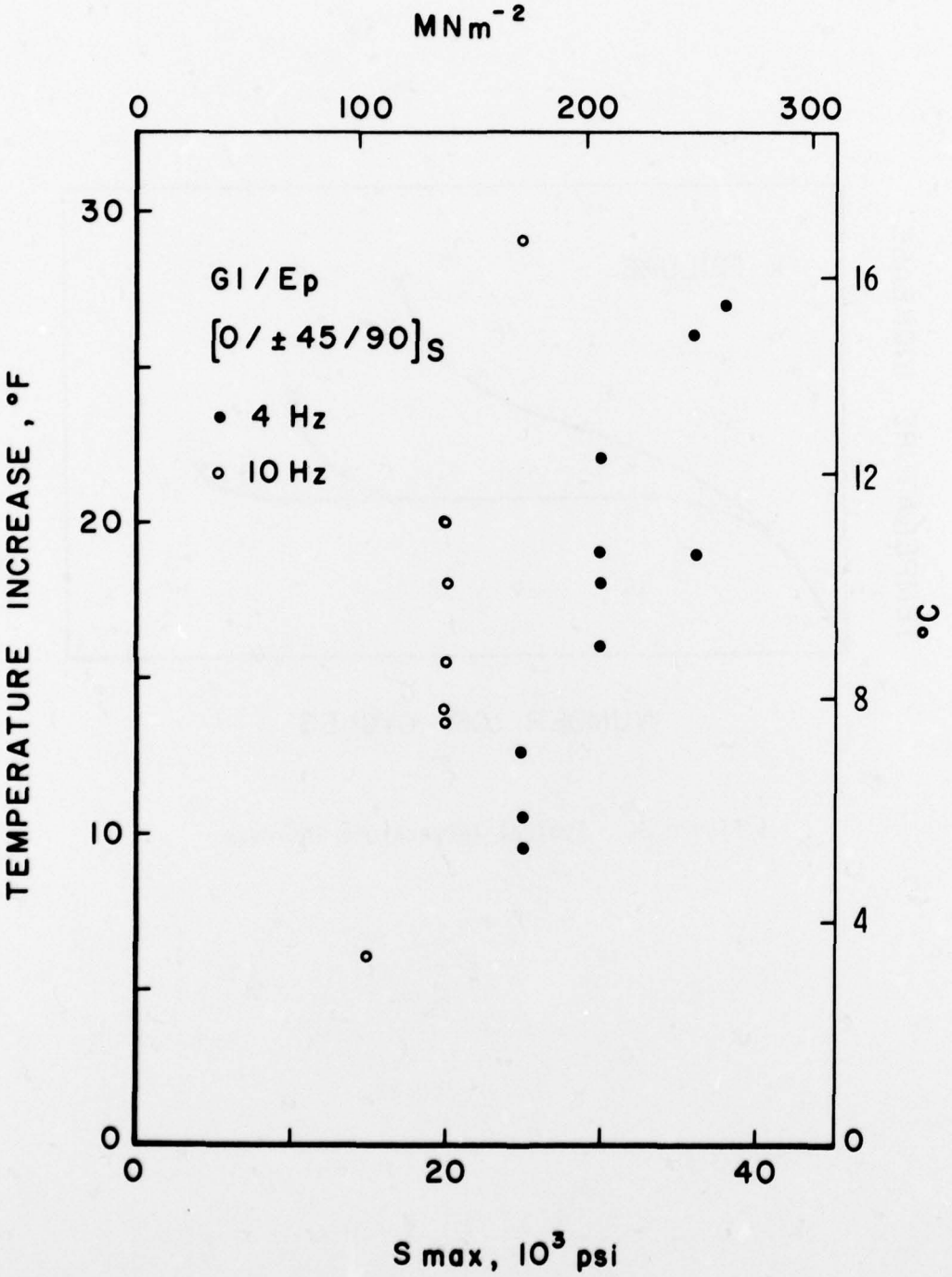

Figure 25. Equilibrium Temperature Increase, $(0/\pm 45/90)_s$ G1/Ep (Reference 54)

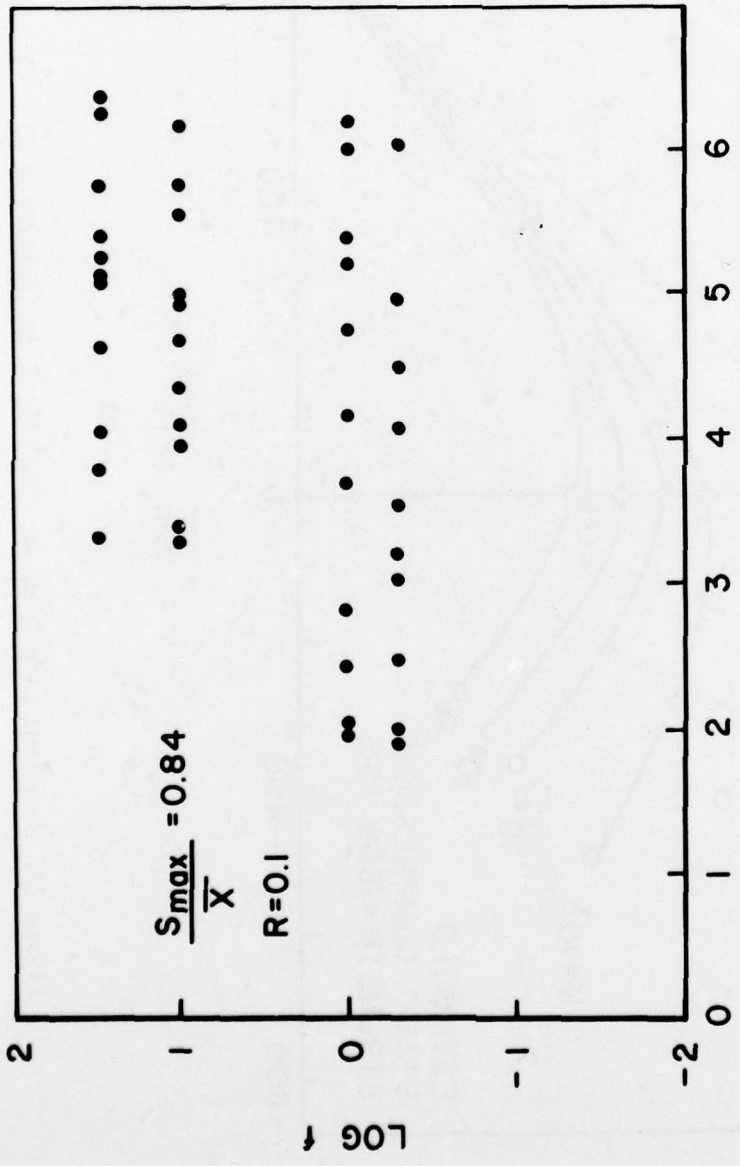

Figure 26. Effect of Frequency f in Hz on Fatigue Life, $(0/\pm45)_S$ Gr/Ep (Reference 60)

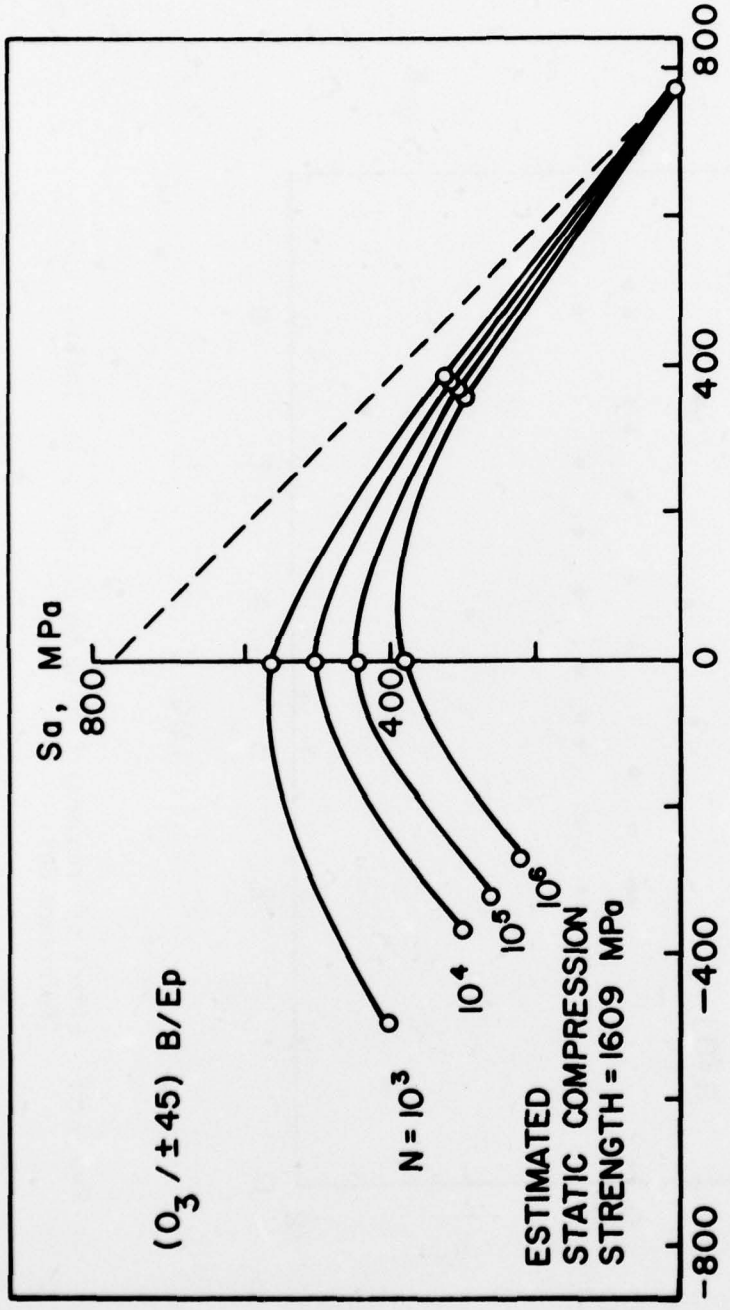

Figure 27. Constant Life Diagram, $(0_3/\pm45)$ B/Ep (Reference 3)

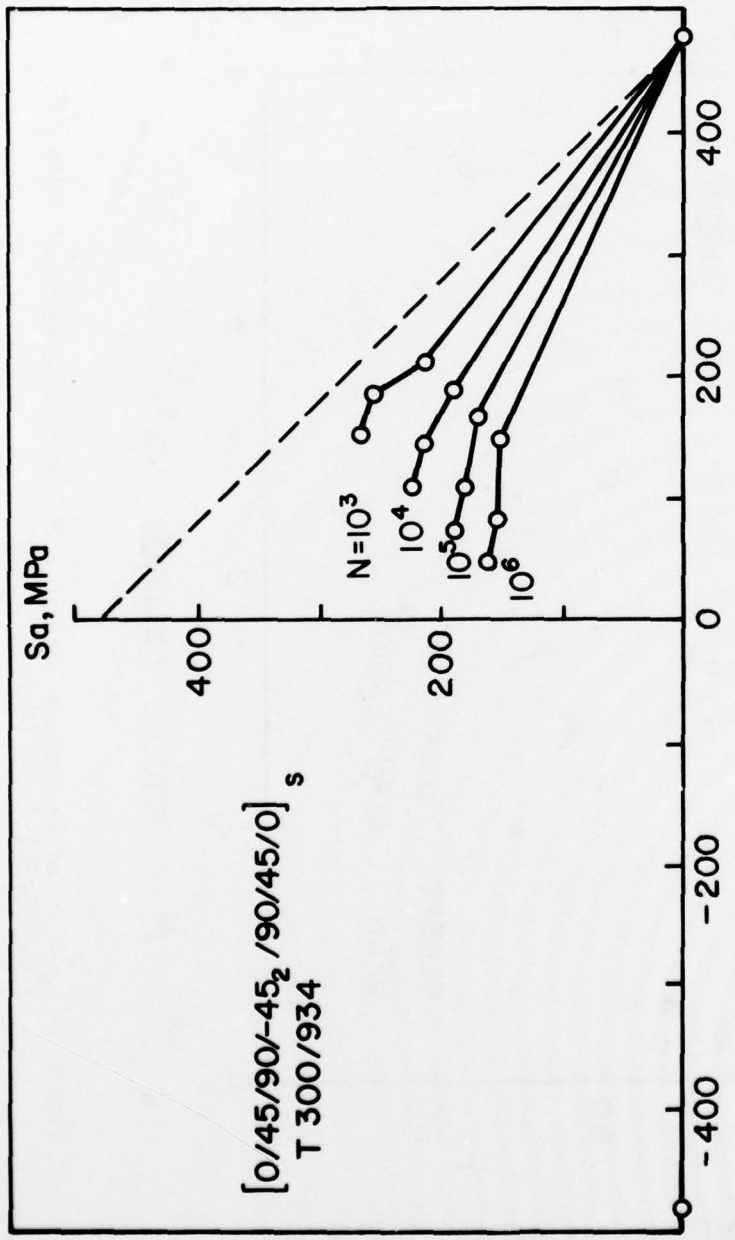

Figure 28. Effect of Compression on Fatigue, (0/±45/90) Gr/Ep (Reference 66)

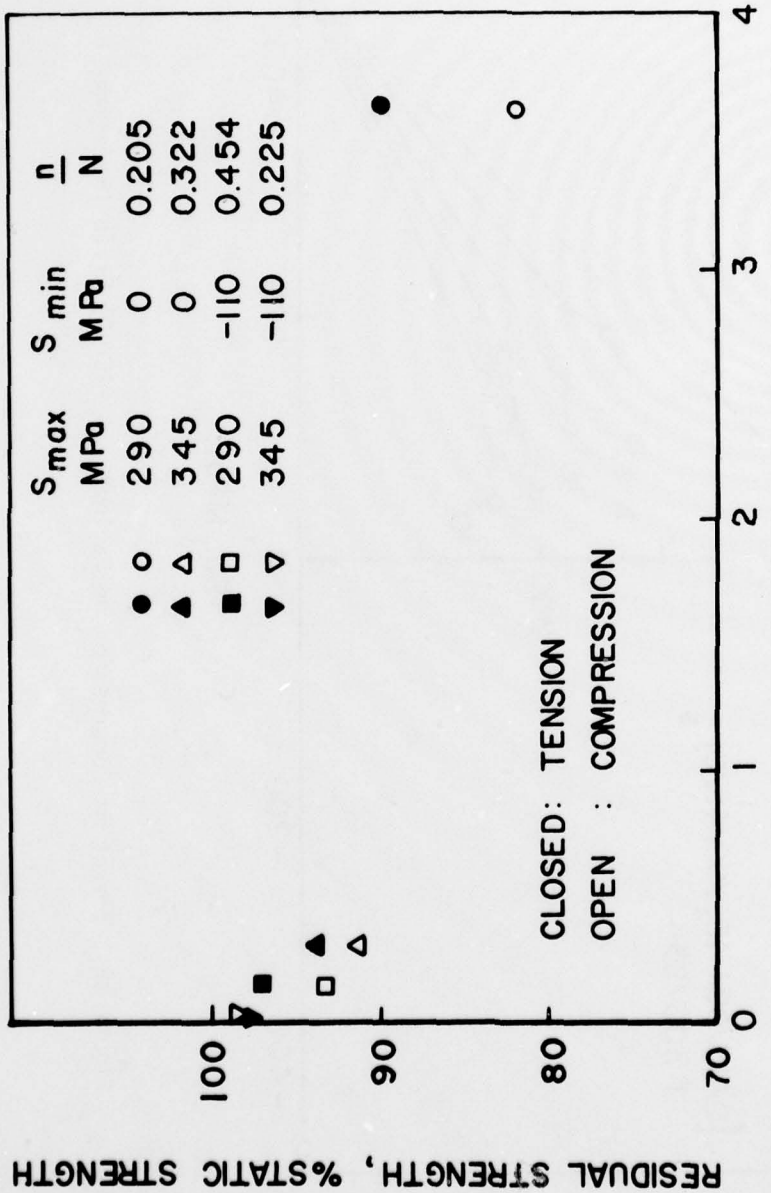

Figure 29. Effect of Fatigue on Tensile and Compressive Residual Strengths (0/±45/90) Gr/Ep (Reference 66)

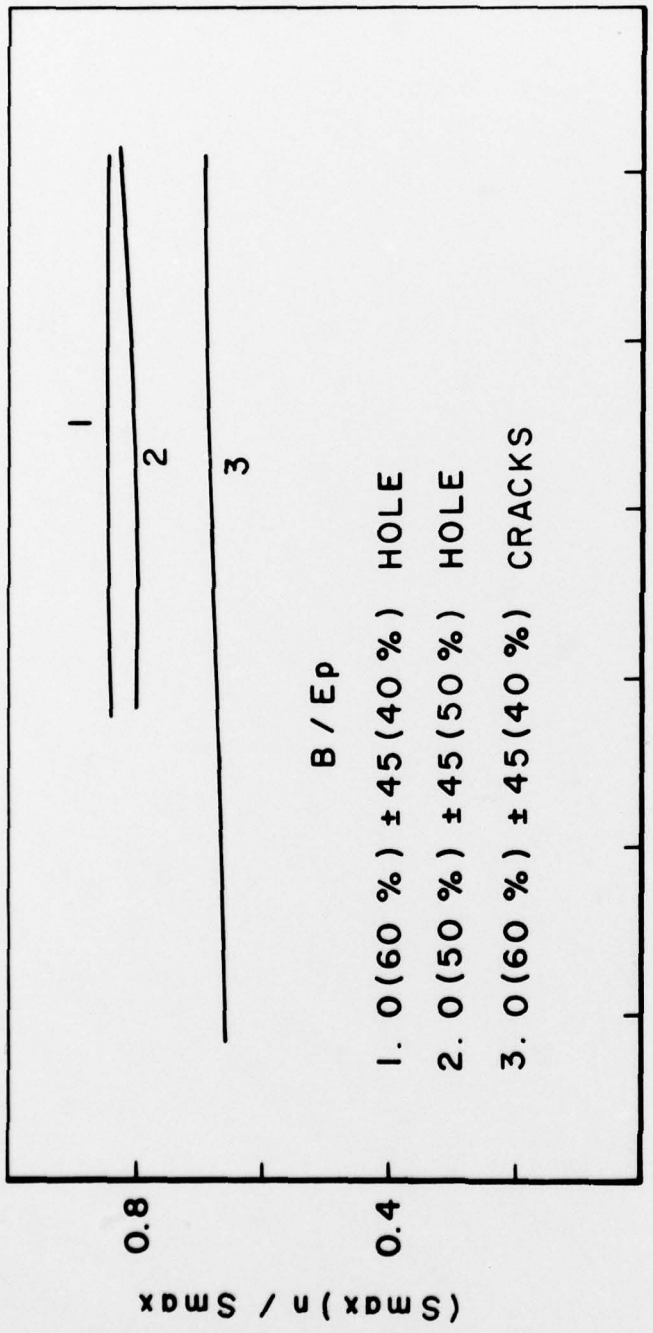

Figure 30. Inverse of Fatigue Notch Factor, B/Ep (Reference 3)

*U.S.Government Printing Office: 1978 — 757-080/113